# Quantum-optical spectroscopy of semiconductors

M. Kira and S. W. Koch
*Department of Physics and Material Sciences Center, Philipps-University Marburg, Renthof 5, D-35032 Marburg, Germany*
(Received 20 September 2005; published 18 January 2006)

The microscopic foundation of quantum-optical spectroscopy is presented. It is proposed to use this technique to generate and detect quasiparticle states in semiconductors whose quantum-statistical properties are governed by that of the exciting light. While resonant classical excitation induces an optical interband polarization, low-intensity quantum excitation directly seeds a quantum-degenerate exciton state which is characterized by long-range order, anomalous reduction of Coulomb and phonon scattering, as well as strongly enhanced and directional quantum emission.

DOI: 10.1103/PhysRevA.73.013813 PACS number(s): 42.50.Ct, 03.75.Kk, 78.47.+p

## I. INTRODUCTION

Optical spectroscopy is a very important and versatile tool for identifying and characterizing elementary processes in a large variety of inorganic [1–5], organic [6,7], and biological [8–10] systems. In many of these applications, it is desirable to use spectrally and/or temporally well-defined sources while the detailed quantum statistics of the exciting light is often not relevant. However, if one carefully characterizes spontaneous emission from excited systems, nonclassical features, such as antibunching [11,12], entanglement [13–15], squeezing [16,17], etc., may show up. The analysis reveals that such effects appear when the light and matter properties cannot be factorized. In other words, quantum-mechanical aspects of the matter excitations influence the quantum statistics of the emitted light via correlations.

If one takes a closer look at the quantum mechanics of optical interactions, one immediately realizes that light-matter correlations may be relevant not only for emission but also for absorption. After all, emission and absorption are fundamentally related processes, especially, when excitations with genuine quantum-light sources are considered. Following up on this notion, we develop the concept of quantum-optical spectroscopy making it possible to map the quantum-statistical properties of the exciting light directly onto the generated state of the quasiparticle excitations in matter.

To illustrate our concept, we study the example of a direct-band-gap semiconductor system where light emission or absorption involves electron-hole-pair excitations. In the usual classical spectroscopy, one excites the system with coherent classical light and monitors the subsequent transmission, reflection, absorption, light scattering, or wave-mixing signatures. These very successful methods continuously reveal a great deal of fascinating many-body physics in semiconductors, ranging from the formation of quasiparticle excitations, their interaction and scattering mechanisms, all the way to disorder features in the particular samples.

However, if one truly wants to explore the full potential of optical spectroscopy, one should not only consider the semiclassical aspects of light-matter interaction but also utilize its quantum-optical properties to expand the possibilities for generating desired quasiparticle states. Since quantized light has bosonic quantum statistics, the most straightforward approach is to seed the analogous quantum statistics to the excited semiconductor state, even though the electrons and holes obey their intrinsic Fermi statistics.

As an example, we consider manipulating the quantum statistics of Coulomb-bound electron-hole pairs, i.e., excitons, because they are the conceptually simplest optically active quasiparticle excitations. The excitonic statistics can be dominated by the fermionic character of the constituent electron and hole or it may be nearly bosonic under suitable, i.e., low-density and -temperature conditions [18]. In particular, we determine how the boson-to-boson mapping functions and how the fermionic substructure of excitons influence the quantum-statistical aspects as the excitation densities are increased. In connection to this, we show that there is an experimentally accessible parameter range where one can seed a quantum-degenerate exciton state with a macroscopic population of one single level.

As in any quantum theory, the complete system Hamiltonian $H$ defines the starting point for our quantum-electrodynamic treatment of optically excited semiconductor systems. Since the derivation of the generally accepted $H$ for semiconductors has been described in the literature [5,19,20], we just briefly summarize these aspects in Sec. II. After the proper $H$ is identified, we evaluate the quantum dynamics of different excitation schemes from the Heisenberg equations of motion for the relevant operator combinations. In particular, we find a closed set of self-consistent equations for the expectation values by applying the so-called cluster-expansion-truncation scheme [21–25] outlined briefly in Sec. II B and Appendix A. The general theory for quantum-optical spectroscopy is derived in Sec. III. As a result, we obtain a full description of the most important quantum-optical excitation properties, which allows us to analyze the principles of quantum-optical spectroscopy of semiconductors. The effect of quantum statistics of light on quasiparticle excitations is solved analytically in Sec. IV by introducing meaningful simplifications to the excitation problem. The full numerical solutions, presented in Sec. V, illustrate the principles of quantum-optical spectroscopy via several relevant examples. These concepts are summarized and extended in Sec. VI.

 

## II. QUANTUM-ELECTRODYNAMIC APPROACH FOR SEMICONDUCTORS

We consider a system with either a quantum well or a planar arrangement of identical quantum wires. In both cases, we assume sufficiently strong quantum confinement so that only two optically active bands exist in the spectral range of interest. The quantum wires are placed such that they are much closer than the relevant optical wavelength but, at the same time, they are so far apart that the different wires are not electronically coupled. In this situation, each quantum wire is electronically independent and optical effects do not lead to a diffraction pattern. Consequently, the quantum-wire arrangement is as close as possible to the quantum well; indeed, such an arrangement behaves qualitatively very similarly to the quantum well (see, e.g., Ref. [25]). As an illustration, we present computational results for the case of a quantum-wire system with typical GaAs material parameters providing 11 meV exciton binding energy and a three-dimensional (3D) Bohr radius of $a_0=12.5$ nm. We study resonant excitation configurations at low temperatures such that only acoustic phonons are relevant.

### A. System Hamiltonian

For semiconductors, the microscopic description of carrier excitations can be obtained with the help of the fermionic operators $a_{c,\mathbf{k}}$ and $a^\dagger_{c,\mathbf{k}}$ for conduction-band electrons and $a_{v,\mathbf{k}}$ and $a^\dagger_{v,\mathbf{k}}$ for valence-band electrons. For notational simplicity, we present the equations in a form compatible with the quantum-well case; reduction to quantum wires is obtained by replacing the vectorial carrier momentum $\mathbf{k}$ by the scalar $k$ along the wire.

Both the quantized light, i.e., photons, and the lattice vibrations, i.e., phonons, influence the dynamics of the quasiparticle excitations in semiconductors. For a quantum-mechanical description of the transverse electromagnetic field, we start from the vector potential $\mathbf{A}$ within the canonical quantization scheme [19]. The quantization procedure gives

$$\mathbf{A}(\mathbf{r},z)=\sum_{\mathbf{q},q_\perp}\mathcal{E}_q/\omega_q[\mathbf{U}_{\mathbf{q},q_\perp}(\mathbf{r})B_{\mathbf{q},q_\perp}+\text{H.c.}] \tag{1}$$

where $\mathcal{E}_q=\sqrt{\hbar\omega_q/(2\epsilon_0)}$ is the so-called vacuum field amplitude, $\omega_q=cq$ is the optical frequency, and $q=\sqrt{|\mathbf{q}|^2+q_\perp^2}$ is the magnitude of the photon wave vector $(\mathbf{q},q_\perp)$ which is divided into the component $q_\perp$ perpendicular to the planar structure and the parallel component $\mathbf{q}$. The bosonic photon operator $B_{\mathbf{q},q_\perp}$ defines the quantum statistics of a light mode $\mathbf{U}_{\mathbf{q},q_\perp}(\mathbf{r})$. The quantized lattice vibrations can be treated similarly to the electromagnetic field by introducing the bosonic operators $D_{\mathbf{p},p_\perp}$ and $D^\dagger_{\mathbf{p},p_\perp}$ for phonons with parallel and perpendicular momenta $\mathbf{p}$ and $p_\perp$, respectively. For photons and phonons, the independent polarization directions are implicitly included into the momentum index.

The fundamental system Hamiltonian $H_{\text{tot}}=H_0+H_C+H_D+H_P$ follows from [5,19,20]

$$\begin{aligned}
H_0&=\sum_{\mathbf{k}}(\epsilon^c_{\mathbf{k}}a^\dagger_{c,\mathbf{k}}a_{c,\mathbf{k}}+\epsilon^v_{\mathbf{k}}a^\dagger_{v,\mathbf{k}}a_{v,\mathbf{k}})+\sum_{\mathbf{q},q_\perp}\hbar\,\omega_q\left(B^\dagger_{\mathbf{q},q_\perp}B_{\mathbf{q},q_\perp}+\frac{1}{2}\right)\\
&\quad+\sum_{\mathbf{p},p_\perp}\hbar\,\Omega_p\left(D^\dagger_{\mathbf{p},p_\perp}D_{\mathbf{p},p_\perp}+\frac{1}{2}\right),\\
H_C&=\frac{1}{2}\sum_{\mathbf{k},\mathbf{k}',\mathbf{q}\neq 0}V_{\mathbf{q}}(a^\dagger_{c,\mathbf{k}+\mathbf{q}}a^\dagger_{c,\mathbf{k}'-\mathbf{q}}a_{c,\mathbf{k}'}a_{c,\mathbf{k}}\\
&\quad+a^\dagger_{v,\mathbf{k}+\mathbf{q}}a^\dagger_{v,\mathbf{k}'-\mathbf{q},}a_{v,\mathbf{k}'}a_{v,\mathbf{k}}+2a^\dagger_{c,\mathbf{k}+\mathbf{q}}a^\dagger_{v,\mathbf{k}'-\mathbf{q}}a_{v,\mathbf{k}'}a_{c,\mathbf{k}}),\\
H_D&=-\sum_{\mathbf{q},q_\perp,\mathbf{k}}i\hbar\,\mathcal{F}_{\mathbf{q}}(a^\dagger_{v,\mathbf{k}}a_{c,\mathbf{k}-\mathbf{q}}+a^\dagger_{c,\mathbf{k}}a_{v,\mathbf{k}-\mathbf{q}})B_{\mathbf{q},q_\perp}+\text{H.c.},\\
H_P&=\sum_{\mathbf{p},p_\perp,\mathbf{k}}[G^c_{\mathbf{p}}(D_{\mathbf{p},p_\perp}+D^\dagger_{-\mathbf{p},p_\perp})a^\dagger_{c,\mathbf{k}}a_{c,\mathbf{k}-\mathbf{p}}\\
&\quad+G^v_{\mathbf{p}}(D_{\mathbf{p},p_\perp}+D^\dagger_{-\mathbf{p},p_\perp})a^\dagger_{v,\mathbf{k}}a_{v,\mathbf{k}-\mathbf{p}}].
\end{aligned}\tag{2}$$

The noninteracting carriers, photons, and phonons are included in $H_0$ and the corresponding carrier energies are

$$\epsilon^c_{\mathbf{k}}=\frac{\hbar^2\mathbf{k}^2}{2m_e}+E_g,\quad \epsilon^v_{\mathbf{k}}=-\frac{\hbar^2\mathbf{k}^2}{2m_h}, \tag{3}$$

with the band-gap energy $E_g$ and the effective electron and hole masses $m_{e,h}$. The phonon dispersion is given by $\Omega_{\mathbf{p}}$. The Coulombic many-body Hamiltonian $H_C$ contains the bare Coulomb matrix element $V_{\mathbf{k}}$ [26] of the confined system. The interaction between the optical photons and carriers follows from $H_D$, and the interaction strength is determined by $\mathcal{F}_{\mathbf{q}}\equiv d_{v,c}U_{\mathbf{q}}\mathcal{E}_{\mathbf{q}}/\hbar$ where $d_{v,c}$ is the dipole-matrix element. The strength of the phonon-carrier interaction $H_P$ is determined by the form factor $G^\lambda_{\mathbf{p}}$ [27].

### B. Formal aspects of semiconductor quantum dynamics

As a general starting point of our investigations, we evaluate the expectation values $\langle O\rangle=\text{Tr}(O\rho)$ for generic operator $O$, according to the probabilistic interpretation of quantum mechanics and solve their dynamics using the Heisenberg equations of motion

$$i\hbar\frac{\partial}{\partial t}\langle O\rangle=\langle[O,H_{\text{tot}}]_-\rangle \tag{4}$$

which generally leads to the well-known hierarchy problem of infinite coupled equations. In the following, we overview briefly how the quantum dynamics of the interacting semiconductor-photon-phonon system can be treated systematically via the so-called cluster expansion [21–25].

This method is based on a general classification scheme where each operator combination is identified via particle clusters. For semiconductor systems, bosonic $B_1$ and $D_2$ as well as fermionic carrier operator pairs $a^\dagger_1a_2$ correspond to single-particle operators; we have used here an implicit notation where numerals 1 and 2 denote the appropriate momentum, polarization, or band index combinations. Then, a general $N$-particle operator follows from $N$

$=B_1^\dagger \cdots B_{N_1}^\dagger D_1^\dagger \cdots D_{N_2}^\dagger a_1^\dagger \cdots a_{N_3}^\dagger a_{N_3} \cdots a_1 D_{N_4} \cdots D_1 B_{N_5} \cdots B_1$ with all possible combinations of $N_j$ where the total number of operators satisfies $N_1+N_2+N_3+N_4+N_5=N$. According to this classification, $H_C$, $H_P$, and $H_D$ correspond to two-particle interactions and the hierarchy problem of semiconductors is cast into the form

$$i\frac{\partial}{\partial t}\langle N\rangle = T[\langle N\rangle] + V[\langle N+1\rangle], \tag{5}$$

where the $N$-particle expectation value $\langle N\rangle$ couples to higher-order $\langle N+1\rangle$ quantities via the functional $V$. The functional $T$ results mainly from the noninteracting part of the Hamiltonian while $V$ originates from the Coulomb, light-matter, and carrier-phonon interactions.

The cluster-expansion truncation is based on a clear physical principle where one determines all consistent factorizations of an $N$-particle quantity $\langle N\rangle$ in terms of (i) independent single particles (singlets), (ii) correlated pairs (doublets), (iii) correlated three-particle clusters (triplets), up to (iv) correlated $N$-particle clusters. If we formally know all expectation values from $\langle 1\rangle$ to $\langle N\rangle$, a specific correlated cluster recursively follows from

$$\langle 2\rangle = \langle 2\rangle_S + \Delta\langle 2\rangle,$$

$$\langle 3\rangle = \langle 3\rangle_S + \langle 1\rangle\Delta\langle 2\rangle + \Delta\langle 3\rangle,$$

$$\langle N\rangle = \langle N\rangle_S + \langle N-2\rangle_S\Delta\langle 2\rangle + \langle N-4\rangle_S\Delta\langle 2\rangle\Delta\langle 2\rangle + \cdots + \Delta\langle N\rangle. \tag{6}$$

Here, the quantities with the subscript $S$ denote the singlet contributions and the terms $\Delta\langle J\rangle$ contain the purely correlated part of the $J$-particle cluster. In Eq. (6), each term includes a sum over all possibilities to reorganize the $N$ coordinates among singlets, doublets, and so on by including the possible sign changes due to the permutations of the carrier operators. This way all cluster groups in Eq. (6) are fully antisymmetric for fermionic carriers and symmetric for bosonic photon and phonon operators, respectively. As examples, the singlet factorization produces the Hartree-Fock factorization for pure carrier operators, while the classical factorization $\langle N\rangle_S=\langle 1\rangle\langle 1\rangle\cdots\langle 1\rangle=\langle 1\rangle^N$ is obtained for pure photon or phonon terms.

The systematic cluster-expansion truncation of the hierarchy problem follows as we present any given $N$-particle quantity up to $C$-particle correlations,

$$\langle N\rangle_{1,\ldots,C} \equiv \langle N\rangle_S + \langle N\rangle_D + \cdots + \langle N\rangle_C = \sum_{J=1}^{C}\langle N\rangle_J, \tag{7}$$

following directly from Eq. (6) by noting that $\langle N\rangle_S$ contains only singlets, $\langle N\rangle_D$ contains all combinations of doublets but no higher-order correlations, and so on. For example, if the electron-hole system contains only bound pairs like excitons, the description up to doublets is sufficient [24,28–30]. If the system develops molecules or droplet correlations [31,32], higher-order clusters need to be included.

When we truncate the hierarchy to the consistent singlet-doublet level and include three-particle contributions at scattering level, we end up with the general equation structure

$$i\hbar\frac{\partial}{\partial t}\langle 1\rangle = T_1[\langle 1\rangle] + V_1[\langle 2\rangle_S] + V_1[\Delta\langle 2\rangle],$$

$$i\hbar\frac{\partial}{\partial t}\Delta\langle 2\rangle = T_2[\Delta\langle 2\rangle] + V_2[\langle 3\rangle_{SD}] + G[\langle 1\rangle,\Delta\langle 2\rangle], \tag{8}$$

where the functional $G[\langle 1\rangle,\Delta\langle 2\rangle]$ indicates that three-particle correlations are included at the scattering level discussed in Appendix A. This seemingly simple formal structure includes the microscopic description for optical excitations of semiconductors including nonlinear classical optics as well as the most relevant aspects of semiconductor quantum optics.

## III. OPTICAL EXCITATION OF SEMICONDUCTORS

The main idea of quantum-optical spectroscopy is to excite different matter states using light with specific quantum statistics. The analysis of the generated quasiparticle states can be performed by monitoring the subsequent quantum emission, which allows us to deduce the resulting quantum dynamics of the matter excitations. To illustrate this concept, we now apply the cluster-expansion formalism to solve optical excitations in the direct-band semiconductor system described by Hamiltonian (2). We are particularly interested in identifying the effects resulting from a given quantum statistics of the exciting light. In general, the quantum statistics of light contains the complete information about the quantum as well as classical aspects of a given optical field. It can be represented in several equivalent ways; here, we classify the field via either its density matrix, wave function, or all possible $(J+K)$-particle expectation values $\langle[B^\dagger]^J B^K\rangle$.

We consider two excitation schemes: (i) classical and (ii) entirely incoherent quantum light with quantum statistics defined by

$$\langle[B^\dagger]^J B^K\rangle|_{\text{classical}} = \langle B^\dagger\rangle^J\langle B\rangle^K,$$

$$\langle[B^\dagger]^J B^K\rangle|_{\text{quantum}} = \delta_{J,K}J!\,\Delta\langle B^\dagger B\rangle^J, \tag{9}$$

respectively. The classical excitation follows from the single-particle quantities and classical factorization whereas pure quantum excitation is characterized by two-particle correlations describing the incoherent quantum fluctuations of the field. One of the reasons for us to choose these two schemes is the possibility to demonstrate the capabilities of quantum-optical spectroscopy in semiconductors because such classical and quantum fields have drastically different quantum statistics. The other reason is that both of these schemes can be realized using currently available experimental setups.

It is interesting to note that the coherent state [19,33]

$$|\beta\rangle \equiv D(\beta)|0\rangle, \quad D(\beta) \equiv e^{\beta^\star B - \beta B^\dagger} \tag{10}$$

corresponds to a classical field since $\langle[B^\dagger]^J B^K\rangle = \langle\beta|[B^\dagger]^J B^K|\beta\rangle = [\beta^\star]^J\beta^K$ produces the classical factoriza-

tion in Eq. (9) after we identify $\beta=\langle B\rangle$. From a quantum-optical point of view, a coherent state—i.e., classical field—is obtained when the coherent displacement operator $D(\beta)$ acts on the vacuum state $|0\rangle$.

We can also find the precise density matrix of the quantum excitation used here; it is given by the thermal state

$$\hat{\rho}_{\rm th}=\sum_{j=0}^{\infty}|j\rangle\frac{n_{\rm th}^{j}}{(1+n_{\rm th})^{j+1}}\langle j|, \tag{11}$$

where $|j\rangle$ is the usual Fock-number state [19,33]. Since this field has $\langle[B^{\dagger}]^{J}B^{K}\rangle=\mathrm{Tr}([B^{\dagger}]^{J}B^{K}\hat{\rho}_{\rm th})=\delta_{J,K}J![n_{\rm th}]^{J}$, the quantum excitation in Eq. (9) is equivalent to $\hat{\rho}_{\rm th}$ after we identify $n_{\rm th}=\Delta\langle B^{\dagger}B\rangle$. There are in fact infinitely many other forms of $\langle[B^{\dagger}]^{J}B^{K}\rangle$ that could be used for the quantum excitation. However, the thermal light is the simplest quantum field and also most easily accessible source in experiments. The role of other quantum excitations is discussed later in Sec. VI after the relation between quantum statistics and quasiparticle excitations in matter has been fully described.

Before the exciting light enters into and interacts with the semiconductor, it is assumed to be completely uncorrelated with the electronic system. Such situations are realized with any excitations that are external with respect to the excited system. Similarly, the phonon system is assumed to be initially uncorrelated with both photons and carriers. As a result, the total density matrix $\hat{\rho}_{\rm tot}$ separates into light, phonon, and electronic parts i.e., $\hat{\rho}_{\rm tot}=\hat{\rho}_{\rm light}\otimes\hat{\rho}_{\rm phonons}\otimes\hat{\rho}_{\rm electrons}$ before the interactions take place. The specific form of $\hat{\rho}_{\rm light}$ follows from Eq. (10) or (11) and the phonon system is chosen to be a thermal bath where phonon occupations follow a Bose-Einstein distribution. The many-body features of the electronic system can be investigated in its purest form when we assume that the semiconductor is in its ground state $|G\rangle$ before the excitation. Thus, we choose $\hat{\rho}_{\rm electrons}=|G\rangle\langle G|$ in our analysis. As the light interacts with the semiconductor, nontrivial electron-photon-phonon correlations build up and are computed self-consistently.

### A. Classical excitation scheme

The classical part of the light field is directly connected to the coherent amplitudes $\langle B_q\rangle$ and $\langle B_q^{\dagger}\rangle$ such that only the electric field

$$\langle E(\mathbf{r},t)\rangle=\sum_{\mathbf{q}}\left[i\mathcal{E}_{\mathbf{q}}\mathbf{U}_{\mathbf{q}}(\mathbf{r})\langle B_{\mathbf{q}}\rangle-i\mathcal{E}_{\mathbf{q}}\mathbf{U}_{\mathbf{q}}^{\star}(\mathbf{r})\langle B_{\mathbf{q}}^{\dagger}\rangle\right] \tag{12}$$

is needed to describe the classical field. In the following, we discuss the singlet-doublet equation structure (8), correlations, and the relevant quasiparticle excitations generated by the classical field. The additional correlations and effects in the realm of quantum fields are discussed in connection with the quantum excitation.

The Heisenberg equation of motion for $\langle E\rangle$ yields the well-known wave equation

$$\left(\nabla^2-\frac{n^2(z)}{c^2}\frac{\partial^2}{\partial t^2}\right)\langle E(z,t)\rangle=\mu_0\frac{\partial^2}{\partial t^2}P(z), \tag{13}$$

where we have assumed that the light field propagates in the $z$ direction perpendicular to a planar structure with the background refractive index $n(z)$. The right-hand side of Eq. (13) shows that the classical light field is directly coupled to the optical polarization $P(z)=g(z)P$ where $g(z)\to\delta(z)$ follows from the strong planar confinement of carriers. The macroscopic polarization $P$ is given by

$$P=\frac{d_{vc}}{\mathcal{S}}\sum_{\mathbf{k}}P_{\mathbf{k}},\quad P=\frac{d_{vc}}{l\mathcal{L}}\sum_{k}P_{k}, \tag{14}$$

for the quantum-well and -wire structures, respectively; the quantization area is given by $\mathcal{S}$ or $l\mathcal{L}$ where $l$ is the separation of wires in the planar arrangement. Since the microscopic polarization follows from a singlet term, $P_{\mathbf{k}}\equiv\langle a_{v,\mathbf{k}}^{\dagger}a_{c,\mathbf{k}}\rangle$, the wave equation contains only single-particle contributions without the hierarchy problem. Thus, Eq. (13) is exact and its accuracy depends only on how precisely we are able to solve $P_{\mathbf{k}}$.

The dynamics of $P_{\mathbf{k}}$ couples to other singlets: $\langle E(z,t)\rangle$, the occupation probabilities of electrons $f_{\mathbf{k}}^{e}\equiv\langle a_{\mathbf{k},c}^{\dagger}a_{\mathbf{k},c}\rangle$ and holes $f_{\mathbf{k}}^{h}\equiv\langle a_{\mathbf{k},v}a_{\mathbf{k},v}^{\dagger}\rangle$. In addition, the beginning of the hierarchy problem appears via the coupling to two-particle correlations. Altogether, the classical excitation leads to the singlet dynamics

$$i\hbar\frac{\partial}{\partial t}P_{\mathbf{k}}\bigg|_{\rm clas}=\tilde{\epsilon}_{\mathbf{k}}P_{\mathbf{k}}-(1-f_{\mathbf{k}}^{e}-f_{\mathbf{k}}^{h})\Omega_{\mathbf{k}}-i\Gamma_{\mathbf{k}}, \tag{15}$$

$$\frac{\hbar}{2}\frac{\partial}{\partial t}f_{\mathbf{k}}^{e}\bigg|_{\rm clas}=\mathrm{Im}\left(P_{\mathbf{k}}\Omega_{\mathbf{k}}^{\star}+\sum_{\mathbf{q},\mathbf{k}',\lambda}V_{\mathbf{q}}c_{c,\lambda,\lambda,c}^{\mathbf{q},\mathbf{k}',\mathbf{k}}+\sum_{\mathbf{q}}\mathcal{D}_{\mathbf{k},\mathbf{q}}^{c,c}\right), \tag{16}$$

$$\frac{\hbar}{2}\frac{\partial}{\partial t}f_{\mathbf{k}}^{h}\bigg|_{\rm clas}=\mathrm{Im}\left(P_{\mathbf{k}}\Omega_{\mathbf{k}}^{\star}-\sum_{\mathbf{q},\mathbf{k}',\lambda}V_{\mathbf{q}}c_{v,\lambda,\lambda,v}^{\mathbf{q},\mathbf{k}',\mathbf{k}}-\sum_{\mathbf{q}}\mathcal{D}_{\mathbf{k},\mathbf{q}}^{v,v}\right), \tag{17}$$

with the renormalized kinetic electron-hole-pair energy and renormalized Rabi frequency

$$\begin{aligned}\tilde{\epsilon}_{\mathbf{k}}&\equiv\epsilon_{\mathbf{k}}^{c}-\epsilon_{\mathbf{k}}^{v}-\sum_{\mathbf{k}'}V_{\mathbf{k}-\mathbf{k}'}(f_{\mathbf{k}'}^{e}+f_{\mathbf{k}'}^{h}),\\ \Omega_{\mathbf{k}}&\equiv d_{cv}E(0,t)+\sum_{\mathbf{k}'}V_{\mathbf{k}-\mathbf{k}'}P_{\mathbf{k}'},\end{aligned} \tag{18}$$

respectively. The last term of Eq. (15) contains the correlated two-particle contributions

$$-i\Gamma_{\mathbf{k}}=\sum_{\mathbf{q}}\left(V_{\mathbf{q}}\sum_{\mathbf{n},\lambda}c_{v,\lambda,\lambda,c}^{\mathbf{q},\mathbf{n},\mathbf{k}}-\mathcal{D}_{\mathbf{k},\mathbf{q}}^{v,c}\right)-(c\leftrightarrow v)^{\star}. \tag{19}$$

The contribution $\Gamma_{\mathbf{k}}$ leads to the dephasing of the polarization via the true two-particle correlations defined from

$$c^{\mathbf{q},\mathbf{k}',\mathbf{k}}_{\lambda,\nu,\nu',\lambda'} \equiv \Delta\langle a^\dagger_{\lambda,\mathbf{k}} a^\dagger_{\nu,\mathbf{k}'} a_{\nu',\mathbf{k}'+\mathbf{q}} a_{\lambda',\mathbf{k}-\mathbf{q}}\rangle$$
$$= \langle a^\dagger_{\lambda,\mathbf{k}} a^\dagger_{\nu,\mathbf{k}'} a_{\nu',\mathbf{k}'+\mathbf{q}} a_{\lambda',\mathbf{k}-\mathbf{q}}\rangle - \langle a^\dagger_{\lambda,\mathbf{k}} a^\dagger_{\nu,\mathbf{k}'} a_{\nu',\mathbf{k}'+\mathbf{q}} a_{\lambda',\mathbf{k}-\mathbf{q}}\rangle_S, \quad (20)$$

where the factorized single-particle contributions are removed. Note that other momentum combinations do not exist for the homogeneous excitation conditions used here. The corresponding phonon terms are defined by

$$\mathcal{D}^{\lambda,\nu}_{\mathbf{k},\mathbf{q}} \equiv \sum_{p_\perp} G^\nu_{\mathbf{q},p_\perp} \Delta\langle (D_{\mathbf{q},p_\perp} + D^\dagger_{-\mathbf{q},p_\perp}) a^\dagger_{\lambda,\mathbf{k}} a_{\nu,\mathbf{k}-\mathbf{q}}\rangle$$
$$= \sum_{p_\perp} G^\nu_{\mathbf{q},p_\perp} [\langle (D_{\mathbf{q},p_\perp} + D^\dagger_{-\mathbf{q},p_\perp}) a^\dagger_{\lambda,\mathbf{k}} a_{\nu,\mathbf{k}-\mathbf{q}}\rangle - \langle D_{\mathbf{q},p_\perp} + D^\dagger_{-\mathbf{q},p_\perp}\rangle \langle a^\dagger_{\lambda,\mathbf{k}} a_{\nu,\mathbf{k}-\mathbf{q}}\rangle]. \quad (21)$$

The set of Eqs. (15)–(17) defines the general *semiconductor Bloch equations*. In addition, one finds quantum-optical corrections of the form $\Delta\langle B^\dagger a^\dagger_1 a_2\rangle$ [20,34–36]. However, these are not relevant for the optical generation of quasiparticles as long as classical excitation is used.

### B. Exciton dynamics after classical excitation

The classical optical excitation induces the coupled dynamics of coherent polarization and densities described by Eqs. (15)–(17). However, the generated $P$ experiences a rather fast decay on a picosecond time scale due to the two-particle correlations described by $\Gamma_{\mathbf{k}}$. The singlet-doublet approach (8) allows us to analyze this decay as the dynamics of the two-particle correlations is worked out. In this context, the exciton correlation determined by $c^{\mathbf{q},\mathbf{k}',\mathbf{k}}_X \equiv c^{\mathbf{q},\mathbf{k}',\mathbf{k}}_{c,v,c,v}$ is the most important long-living correlation. The explicit form of its dynamics follows from [24,28,37]

$$i\hbar \frac{\partial}{\partial t} c^{\mathbf{q},\mathbf{k}',\mathbf{k}}_X = \epsilon^{\mathbf{q},\mathbf{k}',\mathbf{k}} c^{\mathbf{q},\mathbf{k}',\mathbf{k}}_X + S^{\mathbf{q},\mathbf{k}',\mathbf{k}} + (1 - f^e_{\mathbf{k}} - f^h_{\mathbf{k}-\mathbf{q}}) \sum_l V_{l-\mathbf{k}} c^{\mathbf{q},\mathbf{k}',l}_X - (1 - f^e_{\mathbf{k}'+\mathbf{q}} - f^h_{\mathbf{k}'}) \sum_l V_{l-\mathbf{k}'} c^{\mathbf{q},l,\mathbf{k}}_X + iG^{\mathbf{q},\mathbf{k}',\mathbf{k}} + D^{\mathbf{q},\mathbf{k}',\mathbf{k}}_{\text{rest}} + T^{\mathbf{q},\mathbf{k}',\mathbf{k}}. \quad (22)$$

The polarization decay $\Gamma_{\mathbf{k}}$ is related to the generation of exciton correlations,

$$iG^{\mathbf{q},\mathbf{k}',\mathbf{k}} = (P^\star_{\mathbf{k}} - P^\star_{\mathbf{k}-\mathbf{q}}) V_{\mathbf{q}} \sum_{\mathbf{n},\lambda} c^{-\mathbf{q},\mathbf{n},\mathbf{k}'}_{v,\lambda,\lambda,c} + (P^\star_{\mathbf{k}} + P^\star_{\mathbf{k}-\mathbf{q}}) \mathcal{D}^{v,c}_{\mathbf{k}',-\mathbf{q}} + (P_{\mathbf{k}'} - P_{\mathbf{k}'+\mathbf{q}}) V_{\mathbf{q}} \sum_{\mathbf{n},\lambda} c^{\mathbf{q},\mathbf{n},\mathbf{k}}_{c,\lambda,\lambda,v} + (P_{\mathbf{k}'} + P_{\mathbf{k}'+\mathbf{q}}) \mathcal{D}^{c,v}_{\mathbf{k},\mathbf{q}}. \quad (23)$$

This source term contains precisely the same $c_{v,\lambda,\lambda,c}$ and $\mathcal{D}^{v,c}$ correlations that led to a decay of $P$ according to Eq. (19).

The other elements of the exciton correlation dynamics consist of the renormalized electron-hole-pair energy

$$\epsilon^{\mathbf{q},\mathbf{k}',\mathbf{k}} \equiv \epsilon^c_{\mathbf{k}-\mathbf{q}} - \epsilon^v_{\mathbf{k}} - \epsilon^c_{\mathbf{k}'} - \epsilon^v_{\mathbf{k}'+\mathbf{q}} - \sum_l V_l [f^e_{\mathbf{k}-\mathbf{q}-l} + f^h_{\mathbf{k}-l} - f^e_{\mathbf{k}'-l} - f^h_{\mathbf{k}'+\mathbf{q}-l}]. \quad (24)$$

The single-particle source originating from the Coulomb interaction has the explicit form

$$S^{\mathbf{q},\mathbf{k}',\mathbf{k}} = V_{\mathbf{k}'+\mathbf{q}-\mathbf{k}} [(1 - f^e_{\mathbf{k}})(1 - f^h_{\mathbf{k}-\mathbf{q}}) f^e_{\mathbf{k}'+\mathbf{q}} f^h_{\mathbf{k}'} - f^e_{\mathbf{k}} f^h_{\mathbf{k}-\mathbf{q}} (1 - f^e_{\mathbf{k}'+\mathbf{q}})(1 - f^h_{\mathbf{k}'})] + V_{\mathbf{k}'+\mathbf{q}-\mathbf{k}} [P^\star_{\mathbf{k}} P_{\mathbf{k}'+\mathbf{q}} (f^h_{\mathbf{k}-\mathbf{q}} - f^h_{\mathbf{k}'}) + P_{\mathbf{k}'} P^\star_{\mathbf{k}-\mathbf{q}} (f^e_{\mathbf{k}} - f^e_{\mathbf{k}'+\mathbf{q}})] + V_{\mathbf{q}} [P^\star_{\mathbf{k}} P_{\mathbf{k}'} (f^h_{\mathbf{k}-\mathbf{q}} - f^e_{\mathbf{k}'+\mathbf{q}}) - P^\star_{\mathbf{k}-\mathbf{q}} P_{\mathbf{k}'+\mathbf{q}} (f^h_{\mathbf{k}'} - f^e_{\mathbf{k}}) - P^\star_{\mathbf{k}-\mathbf{q}} P_{\mathbf{k}'} (f^e_{\mathbf{k}} - f^e_{\mathbf{k}'+\mathbf{q}}) + P^\star_{\mathbf{k}} P_{\mathbf{k}'+\mathbf{q}} (f^h_{\mathbf{k}'} - f^h_{\mathbf{k}-\mathbf{q}})]. \quad (25)$$

This equation has a rather intuitive interpretation since it contains the usual Boltzmann scattering of carriers, $f_1 f_2 (1 - f_3)(1 - f_4) - (1 - f_1)(1 - f_2) f_3 f_4$, in the first part and nonlinear polarization scattering in the remaining terms. We have also presented explicitly the Coulomb sums with the phase-space filling factor $(1 - f^e - f^h)$ since they describe the attractive interaction between electrons and holes allowing them to become truly bound electron-hole pairs, i.e., *incoherent excitons*. If the carrier density is low enough, the polarization can be efficiently converted into incoherent excitons as shown; for a more detailed discussion, see also Refs. [25,37].

Besides the contributions discussed so far, Eq. (22) also contains a large number of additional terms which are presented here only symbolically. The remaining two-particle contributions denoted as $D_{\text{rest}}$ include, e.g., Coulomb sums of the generic form $\Delta\langle 2\rangle \Sigma V \langle 1\rangle$ or $\langle 1\rangle \Sigma V \Delta\langle 2\rangle$ where the sums involve either single-particle quantities or two-particle correlations, respectively. The first group leads to microscopical Coulomb screening effects in the single-particle terms via their hierarchical coupling to the two-particle correlations. The second group includes, e.g., the Coulomb scattering of one electron or hole inside an exciton with another electron, hole, or with an interband coherence. These terms, together with the phase-space filling, influence how much the fermionic substructure of excitons compromises the accumulation of exciton populations for the given excitation condition. Also coupling to other two-particle carrier, photon, and phonon correlations are included in $D_{\text{rest}}$. The explicit form of the quantum-optical correlations is discussed in connection with our analysis of the quantum excitation below.

In addition to the two-particle correlations, Eq. (22) contains also three-particle correlation terms symbolized by $T^{\mathbf{q},\mathbf{k}',\mathbf{k}}$, which are treated here at the scattering level. These terms describe, e.g., the phonon scattering leading to the formation and equilibration of excitons under incoherent excitation conditions. For a detailed form of the phonon scattering terms, see Refs. [24,27].

#### 1. Excitons and pair-correlation function

Since our approach fully includes the nonbosonic aspects of excitons [5,18], we can directly evaluate how strongly the fermionic phase-space filling as well as the Coulomb and

phonon scattering compromise the generation of excitons. Thus, it is always interesting to project exciton population correlations from the full computations including the complete excitonic dynamics (22). This can be performed precisely by applying the exciton transformation (B4) discussed in Appendix B in more detail. Thus, we can determine the momentum distribution and density [24,28] of a specific exciton state $\nu$ by using

$$\Delta N_\nu(\mathbf{q}) \equiv \Delta\langle X^\dagger_{\nu,\mathbf{q}} X_{\nu,\mathbf{q}}\rangle = \sum_{\mathbf{k},\mathbf{k}'} \phi^L_\nu(\mathbf{k})\phi^L_\nu(\mathbf{k}')c_X^{\mathbf{q},\mathbf{k}'-\mathbf{q}_h,\mathbf{k}+\mathbf{q}_e},$$

$$\Delta n_\nu = \frac{1}{\mathcal{L}^d}\sum_{\mathbf{q}} \Delta N_\nu(\mathbf{q}). \tag{26}$$

The physical relevance of these quantities becomes apparent, e.g., in teraherz (THz) spectroscopy [25,28,38,37–39] where the linear THz absorption measures $\Delta n_\nu$. This is in full analogy to the determination of the atom density via optical absorption spectroscopy in atomic systems.

For our analysis of the excited semiconductor state, it is often useful to investigate the pair-correlation function

$$g(\mathbf{r}) \equiv \Delta\langle P^\dagger(\mathbf{r})P(0)\rangle, \quad P(\mathbf{r}) \equiv \frac{1}{\mathcal{S}}\sum_{\mathbf{k},\mathbf{k}'} a^\dagger_{v,\mathbf{k}} a_{c,\mathbf{k}'} e^{i(\mathbf{k}'-\mathbf{k})\cdot\mathbf{r}}, \tag{27}$$

where $P(\mathbf{r})$ annihilates an electron-hole pair at position $\mathbf{r}$ and $g(\mathbf{r})$ contains just the two-particle correlation. This function basically tells us how an electron-hole pair at position $\mathbf{r}$ is correlated with another pair at $\mathbf{r}'=\mathbf{0}$. Thus, the spatial extension of $g(\mathbf{r})$ into large distances implies that electron-hole-pair correlations exhibit long-range order. From a practical point of view, $g(\mathbf{r})$ is a two-particle quantity that can be evaluated exactly from the doublet correlations by using

$$g(\mathbf{r}) = \frac{1}{\mathcal{S}^2}\sum_{\mathbf{k},\mathbf{k}',\mathbf{q}} c_X^{\mathbf{q},\mathbf{k}',\mathbf{k}} e^{-i\mathbf{q}\cdot\mathbf{r}}, \tag{28}$$

after Eq. (20) is implemented.

### C. Quantum excitation scheme

In the classical excitation scheme, one assumes semiconductor excitation with coherent light that is fully defined by its singlet part $\langle B_{\mathbf{q},q_\perp}\rangle$. The related semiconductor dynamics is discussed in Secs. III A and III B. A purely quantum-mechanical excitation is realized for fields whose classical parts vanish, i.e., where $\langle B_{\mathbf{q},q_\perp}\rangle=0$. In the following, we concentrate on the simplest and most easily reachable quantum excitation described entirely by its photon-number-like fluctuations $\Delta\langle B^\dagger_{\mathbf{q},q_\perp} B_{\mathbf{q}',q'_\perp}\rangle$ while its quantum statistics is thermal, i.e., $\langle [B^\dagger]^J B^K\rangle = \delta_{J,K} J! [\Delta\langle B^\dagger B\rangle]^J$. Before we analyze details of the semiconductor correlations resulting from true quantum excitation, we first identify the parameter combinations for which the relevant aspects—like intensity, temporal, and spectral features—are equal for quantum and classical optical fields.

The initial classical field is defined by $\langle E(z)\rangle = \langle E_0(z)\rangle + \langle E_0^\star(z)\rangle$ and it propagates according to the wave equation (13). As discussed in Appendix C, initial classical and quantum fields have an identical intensity (but different quantum statistics) if

$$\mathcal{E}_q\mathcal{E}_{q'}\Delta\langle B^\dagger_{\mathbf{q},q_\perp} B_{\mathbf{q},q'_\perp}\rangle = \frac{1}{\mathcal{L}}F(\mathbf{q})\langle E_0^\dagger(q_\perp)\rangle\langle E_0(q'_\perp)\rangle,$$

$$\frac{1}{\mathcal{S}}\sum_{\mathbf{q}} F(\mathbf{q}) = 1, \tag{29}$$

where $F(\mathbf{q})$ defines the angular spread of the pure quantum field and $\langle E_0(q_\perp)\rangle \equiv \int dz \langle E_0(z)\rangle e^{-iq_\perp z}$. In this paper, we assume quantum excitation into an angular window determined by $|\mathbf{q}| < \Delta q$ where $\Delta q = (\omega_0/c)\sin\Delta\theta$ is defined by the central energy of the light $\hbar\omega_0 = 1.485$ eV and the angular resolution $\Delta\theta$ of the excitation. For this configuration, $F(\mathbf{q}) = (4\pi/\Delta q^2)\theta(\Delta q - |\mathbf{q}|)$. As the material parameters are inserted, we find that the full 90° optical window corresponds to the maximum in-plane photon momentum $q_0 a_0 = 0.094$ presented in the excitonic units. In the computations, we use either $\Delta\theta = 45°$ or $\Delta\theta = 90°$. The spectral and temporal properties of the excitation are chosen to be either pulsed Gaussian excitation or quasicontinuous wave (cw) quantum pumps determined by

$$\langle E_0(q)\rangle_{\text{pulsed}} = E_0 e^{-(q-q_0)^2/\Delta Q^2} e^{-iqz_0},$$

$$\langle E_0(q)\rangle_{\text{cw}} = \frac{E_0 e^{-iqz_0}}{\sinh[(q-q_0)/\Delta Q + i\gamma_{\text{cw}}]}, \tag{30}$$

respectively. The spectral width and the temporal duration of the excitation is defined by $\Delta Q$, its central frequency is given by $\omega_0 = cq_0$, the intensity is controlled by $|E_0|^2$, $z_0$ defines the initial peak position of the excitation chosen to be far away from the planar semiconductor structure, and the switch on of the quasi-cw excitation follows from $\gamma_{\text{cw}}$. In general, we tested several spectral shapes and also released the condition (29), implying Fourier-limited spectroscopy. In all cases studied, the essential features of the quantum excitation were unchanged.

#### 1. Semiconductor luminescence equations

As a first step of the quantum excitation, we need to propagate the quantum light field toward the planar structure in order to generate quasiparticle excitations. The self-consistent propagation of the quantum light follows from the Heisenberg equation of motion determined for a doublet correlation

$$\frac{\partial}{\partial t}\Delta\langle B^\dagger_{\mathbf{q},q_\perp} B_{\mathbf{q},q'_\perp}\rangle = i(\omega_q - \omega_{q'})\Delta\langle B^\dagger_{\mathbf{q},q_\perp} B_{\mathbf{q},q'_\perp}\rangle + \sum_{\mathbf{k}} (\mathcal{F}_q \Pi^\star_{\mathbf{k},\mathbf{q},q'_\perp} + \mathcal{F}^\star_{q'}\Pi_{\mathbf{k},\mathbf{q},q_\perp}). \tag{31}$$

This equation couples the quantum fluctuations of the light to the photon-assisted polarization $\Pi_{\mathbf{k},\mathbf{q},q_\perp} \equiv \Delta\langle B^\dagger_{\mathbf{q},q_\perp} a^\dagger_{v,\mathbf{k}} a_{c,\mathbf{k}+\mathbf{q}}\rangle$ which is the unfactorizable photon-electron-hole-pair corre-

lation. The strength of the coupling follows from $\mathcal{F}_q \equiv d_{vc}\mathcal{E}_q U_q/\hbar$. Clearly, this equation involves only two-particle correlations. Thus, Eq. (31) is exact and the quality of the solutions depends on how accurately we can describe $\Pi_{\mathbf{k},\mathbf{q},q_\perp}$.

The quantum statistics of the light becomes critically important as we investigate how it excites the matter. In order to solve this quantum excitation problem, we have to evaluate the dynamics of the photon-assisted polarization. As we derive the Heisenberg equations of motion for $\Pi$ and apply the cluster-expansion truncation (8), we obtain

$$\frac{\partial}{\partial t}\Pi_{\mathbf{k},\mathbf{q},q_\perp} = \frac{1}{i\hbar}\Big((\tilde{\epsilon}_{\mathbf{k},\mathbf{q}} - \hbar\omega_q)\Pi_{\mathbf{k},\mathbf{q},q_\perp} - (1 - f^e_{\mathbf{k}+\mathbf{q}} - f^h_{\mathbf{k}}) \times \sum_l V_{\mathbf{k}-l}\Pi_{l,\mathbf{q},q_\perp}\Big) + \mathcal{F}_q\Big(f^e_{\mathbf{k}+\mathbf{q}} f^h_{\mathbf{k}} + \sum_l c_X^{\mathbf{q},\mathbf{k},l}\Big) - (1 - f^e_{\mathbf{k}+\mathbf{q}} - f^h_{\mathbf{k}})\Delta\langle B^\dagger_{\mathbf{q},q_\perp} B_{\mathbf{q}_\Sigma}\rangle - T^\Pi_{\mathbf{k},\mathbf{q},q_\perp} \quad (32)$$

where we have defined the renormalized kinetic energy and introduced an effective photon operator which includes all photons with in-plane momentum $\mathbf{q}$,

$$\tilde{\epsilon}_{\mathbf{k},\mathbf{q}} = \epsilon^c_{\mathbf{k}+\mathbf{q}} - \epsilon^v_{\mathbf{k}} - \sum_l V_{\mathbf{k}-l}(f^e_{l+\mathbf{q}} + f^h_l), \quad B_{\mathbf{q}_\Sigma} \equiv \sum_{q_\perp} \mathcal{F}_{\mathbf{q},q_\perp} B_{\mathbf{q},q_\perp}. \quad (33)$$

The remaining triplet-scattering term $T^\Pi_{\mathbf{k},\mathbf{q},q_\perp}$ is presented only symbolically; its explicit form can be found in Refs. [20,40]. If both quantum and classical fields are present simultaneously, Eq. (33) obtains additional coherent correlation contributions of the type $\Delta\langle B a^\dagger_c a_c\rangle$ as discussed in Refs. [20,34–36]. For the pure quantum excitation, such contributions are not present.

In general, Eqs. (31) and (32) define the fundamental structure of the *semiconductor luminescence equations*. These equations show that $\Pi$ is generated either via the $\Delta\langle B^\dagger B\rangle$ term or via the spontaneous term including the electron-hole plasma source ($f^e f^h$) as well as the exciton-correlation contribution. As the quantum excitation generates $\Pi$, it also seeds exciton correlations via

$$\frac{\partial}{\partial t} c_X^{\mathbf{q},\mathbf{k}',\mathbf{k}}\Big|_{\text{inc}} = -(1 - f^e_{\mathbf{k}} - f^h_{\mathbf{k}-\mathbf{q}})\Pi_{\mathbf{k}',\mathbf{q}\Sigma} - (1 - f^e_{\mathbf{k}'+\mathbf{q}} - f^h_{\mathbf{k}'})\Pi^\star_{\mathbf{k}-\mathbf{q},\mathbf{q}\Sigma}, \quad (34)$$

where $\Pi_{\mathbf{k}',\mathbf{q}\Sigma}$ contains the total $B_{\mathbf{q}_\Sigma}$. The full equation for $(\partial/\partial t)c_X^{\mathbf{q},\mathbf{k}',\mathbf{k}}$ is obtained by including the other parts described in Eq. (22).

From Eq. (26), we see that $\mathbf{q}$ plays the role of the center-of-mass momentum of excitons in $c_X^{\mathbf{q},\mathbf{k}',\mathbf{k}}$. At the same time, $\mathbf{q}$ appears as in-plane photon momentum in the $\Pi$ terms on the right-hand side of Eq. (34). Thus, the photon and exciton momenta have to match once excitons are generated by the quantum excitation. Since the photon momentum is very small, the exciton correlations couple to the incoherent light field only when their center-of-mass momentum $\mathbf{q}$ is nearly vanishing. This selectivity exists only for excitons and not for the carrier densities since their quantum dynamics follows from

$$\frac{\partial}{\partial t} f^e_{\mathbf{k}}\Big|_{\text{inc}} = -2\text{Re}\Big(\sum_{\mathbf{q}} \Pi_{\mathbf{q}\Sigma,\mathbf{k}-\mathbf{q}}\Big),$$

$$\frac{\partial}{\partial t} f^h_{\mathbf{k}}\Big|_{\text{inc}} = -2\text{Re}\Big(\sum_{\mathbf{q}} \Pi_{\mathbf{q}\Sigma,\mathbf{k}}\Big). \quad (35)$$

This general form shows that the carrier momentum $\mathbf{k}$ can have any value and is not limited by the photon momentum $\mathbf{q}$.

To find a closed set of equations for the quantum excitation, one also has to solve, e.g., $c_{c,c,c,c}$ and $c_{v,v,v,v}$ correlations as well as the phonon-assisted correlations appearing in the carrier dynamics (16),(17). Since these contributions are not directly involved in the quantum-excitation dynamics, we do not elaborate the corresponding equation structure here. In general, we numerically solve the full set of equations including the semiconductor luminescence and Bloch equations with the microscopic Coulomb and phonon scattering. Since the focus of this paper is to investigate the effect of quantum statistics on semiconductor excitations, we have presented only those equations that are relevant for this aspect; the remaining parts can be found in Refs. [20,24,28,34,37,40].

## IV. ANALYTIC SOLUTIONS OF QUASIPARTICLE EXCITATIONS

In order to illustrate the major features of classical and quantum excitation spectroscopy, we look for analytic insights by introducing few simplifications which do not compromise the qualitative characteristics of the problem. For homogeneous excitation, the carrier excitations satisfy the general relations

$$\langle a^\dagger_{\lambda,\mathbf{k}} a_{\lambda',\mathbf{k}'}\rangle = \delta_{\mathbf{k},\mathbf{k}'}\langle a^\dagger_{\lambda,\mathbf{k}} a_{\lambda',\mathbf{k}}\rangle,$$

$$\Delta\langle a^\dagger_{\lambda,\mathbf{k}} a^\dagger_{\lambda',\mathbf{k}'} a_{\nu',\mathbf{k}'+\mathbf{q}'} a_{\nu,\mathbf{k}+\mathbf{q}}\rangle = \delta_{\mathbf{q},\mathbf{q}'} c^{\mathbf{q},\mathbf{k}',\mathbf{k}}_{\lambda,\lambda',\nu',\nu}. \quad (36)$$

In this situation, polarization, exciton correlation, and photon-assisted polarization can be projected into the exciton basis by using the transformations

$$p_\lambda = \sum_{\mathbf{k}} \phi^L_\lambda(\mathbf{k}) P_{\mathbf{k}}, \quad P_{\mathbf{k}} = \sum_\lambda p_\lambda \phi^R_\lambda(\mathbf{k}),$$

$$\Delta\langle X^\dagger_{\lambda,\mathbf{q}} X_{\nu,\mathbf{q}}\rangle = \sum_{\mathbf{k},\mathbf{k}'} \phi^L_\lambda(\mathbf{k})\phi^L_\nu(\mathbf{k}') c_X^{\mathbf{q},\mathbf{k}'-\mathbf{q}_h,\mathbf{k}+\mathbf{q}_e},$$

$$c_X^{\mathbf{q},\mathbf{k}'-\mathbf{q}_h,\mathbf{k}+\mathbf{q}_e} = \sum_{\lambda,\nu} \phi^R_\lambda(\mathbf{k})\phi^R_\nu(\mathbf{k}')\Delta\langle X^\dagger_{\lambda,\mathbf{q}} X_{\nu,\mathbf{q}}\rangle,$$

$$\Pi_{\lambda,0,q_\perp} = \sum_{\mathbf{k}} \phi^L_\lambda(\mathbf{k})\Pi_{\mathbf{k},0,q_\perp}, \quad \Pi_{\mathbf{k},0,q_\perp} = \sum_{\lambda} \Pi_{\lambda,0,q_\perp}\phi^R_\lambda(\mathbf{k}). \tag{37}$$

The dynamics of these is given by Eqs. (B5) and (B6) for classical excitation and by Eqs. (B9) and (B10) for quantum excitation; see Appendix B for more details.

For our analytic considerations, we simplify the light-propagation problem by neglecting the self-consistent back coupling of the excitation to the polarization or photon-assisted polarization in Eqs. (13) and (31). This way, the light field is determined externally while the reemission from the quantum-well or -wire system is omitted. This is clearly not a critical approximation since the reemission usually does not much influence the excitation dynamics unless optical feedback, as in a cavity, becomes important. Since we are interested to determine the characteristics of the state that is directly generated by the excitation, we also neglect the subsequent scattering mechanisms.

### A. Classical excitations

Under these conditions, the classical excitation is described by Eqs. (16), (17), (B5), and (B6) in Appendix B. Especially, Eq. (B5) shows that one dominantly generates $1s$ polarization when the excitation frequency coincides with the $1s$-exciton resonance. This argument is supported further by noting that $\phi_{1s}(\mathbf{r}=\mathbf{0})$ is an order of magnitude larger than any other exciton state [5]. With these simplifications, Eqs. (16), (17), (B5), and (B6) reduce to

$$i\hbar\frac{\partial}{\partial t}p_{1s} = E_{1s}p_{1s} - d_{vc}\phi^R_{1s}(\mathbf{r}=\mathbf{0})\langle E(t)\rangle - i\Gamma_{1s},$$

$$\frac{\hbar}{2}\frac{\partial}{\partial t}f^e_{\mathbf{k}} = \frac{\hbar}{2}\frac{\partial}{\partial t}f^h_{\mathbf{k}} = \mathrm{Im}(P_{\mathbf{k}}\Omega^\star_{\mathbf{k}}),$$

$$i\hbar\frac{\partial}{\partial t}\Delta\langle X^\dagger_{1s,\mathbf{q}}X_{1s,\mathbf{q}}\rangle = +iG^{1s,1s}(\mathbf{q}), \tag{38}$$

where we have omitted the additional scattering terms for simplicity and used $P_{\mathbf{k}}=p_{1s}\phi^R_{1s}(\mathbf{k})$. Equation (38) indicates that classical excitation directly generates polarization and carrier densities which are both single-particle quantities. True exciton populations are generated only via polarization-to-population scattering described by $\Gamma$ and $G$. Thus, the classical excitation intrinsically induces only single-particle quantities.

### B. Quantum excitations

The features of quantum excitation can be accessed by introducing an exciton basis. For simplicity, we assume that the excitation involves only light propagating in the perpendicular direction, i.e., $F(\mathbf{q})=\mathcal{S}\delta_{\mathbf{q},0}$. The analysis in Appendix B shows that only the state

$$\Delta\langle X^\dagger_{\lambda,\mathbf{q}}X_{\nu,\mathbf{q}}\rangle = \delta_{\lambda,\nu}\delta_{\lambda,1s}\delta_{\mathbf{q},0}\Delta\langle X^\dagger_{1s,0}X_{1s,0}\rangle = \delta_{\lambda,\nu}\delta_{\lambda,1s}\delta_{\mathbf{q},0}\Delta N_{1s}(0) \tag{39}$$

is generated and all other correlations are vanishingly small for resonant quantum excitation. In addition, the essential features of the quantum excitation Eqs. (32), (34), and (35) are shown to follow from

$$\frac{\partial}{\partial t}\Pi_{1s,0,q_\perp} = i\left(\omega_{q_\perp} - \frac{1}{\hbar}E_{1s}\right)\Pi_{1s,0,q_\perp} - \phi^R_{1s}(\mathbf{r}=\mathbf{0})\Delta\langle B^\dagger_{0,q_\perp}B_{0_\Sigma}\rangle - T^\Pi_{\mathbf{k},0,q_\perp}, \tag{40}$$

$$\frac{\partial}{\partial t}f^e_{\mathbf{k}} = \frac{\partial}{\partial t}f^h_{\mathbf{k}} = -2\mathrm{Re}[\Pi_{1s,0,\Sigma}\phi^R_{1s}(\mathbf{k})], \tag{41}$$

$$\hbar\frac{\partial}{\partial t}\Delta\langle X^\dagger_{1s,\mathbf{q}}X_{1s,\mathbf{q}}\rangle = -2\delta_{\mathbf{q},0}\mathrm{Re}[\phi^R_{1s}(\mathbf{r}=\mathbf{0})\Pi_{1s,0,\Sigma}], \tag{42}$$

where only those scattering terms are written explicitly that contribute to the generation of excitation.

We notice a critical difference between classical and quantum excitation; while classical excitation does not directly generate an exciton population, the quantum excitation scheme directly seeds excitons into the $\mathbf{q}=\mathbf{0}$ state. Thus, the quantum excitation bypasses the polarization-to-population conversion. As an even more intriguing feature, Eqs. (41) and (42) suggest that each exciton occupies the lowest-momentum exciton state since

$$\frac{\partial}{\partial t}\sum_{\mathbf{k}} f^e_{\mathbf{k}}\bigg|_{\mathrm{inc}} = \frac{\partial}{\partial t}\sum_{\mathbf{k}} f^h_{\mathbf{k}}\bigg|_{\mathrm{inc}} = \frac{\partial}{\partial t}\Delta\langle X^\dagger_{1s,0}X_{1s,0}\rangle, \tag{43}$$

i.e., the generated number of excitons equals the total number of generated electrons or holes. This means that the quantum excitation induces a quantum-degenerate exciton state or equivalently an exciton condensate with a singular population of the lowest exciton state.

## V. FULL NUMERICAL ANALYSIS OF QUANTUM-DEGENERATE EXCITON STATE

The analytical discussion of classical and quantum excitations gives us direct insights into the nature of the semiconductor quasiparticle state generated by light with a given quantum statistics. However, such investigations cannot reveal the importance and influence of the scattering and effects due to underlying electronic structure of quasiparticles on that state. Since scattering and phase-space filling effects are unavoidable in semiconductor systems, the corrections and modifications of the analytical results have to be determined by solving the full equations numerically. For that purpose, we perform a full numerical analysis using the complete set of equations describing quantum-optical excitations in semiconductors.

The numerically solved singlet-doublet equations with triplet scattering lead to a closed set of equations consisting of the semiconductor Bloch and luminescence equations as well as the carrier-carrier, carrier-photon, and carrier-phonon

correlation dynamics discussed in Sec. III. In practice, these computations constitute a large set of coupled first-order integro-differential equations which contain nonlinear sources as well as several Coulomb-, photon- and phonon-interaction-induced integrals. We solve the full excitation dynamics for a homogeneously excited quantum-wire system such that the condition (36) is strictly satisfied. Since the phonons exist in the entire semiconductor, not only in the low-dimensional structure, it is reasonable to assume that phonons act as a bath where the occupation of the phonon states follows from a Bose-Einstein distribution at the lattice temperature. The generated phonon-carrier correlations and scattering terms are evaluated in the Markov limit as discussed in Appendix A. See also Refs. [24,27] for details of the phonon scattering. The evaluation of the Coulomb as well as the scattering integrals or sums consumes most of the computation time such that special care is taken to design a numerically feasible discretization grid. An accurate numerical solution is found by discretizing all single-particle quantities and correlations with respect to their photon, phonon, and/or carrier momenta around the physically relevant ranges. In a typical calculation, one needs carrier momenta up to $k_{\max}a_0=4$, and photon energies within a 30 meV energy window around the $1s$ resonance. For a typical calculation, momenta are discretized into about 100 parts; this means that, e.g., the excitonic correlations have $10^6$ complex-valued elements. The resulting discrete set of equations are solved with the fourth-order Runge-Kutta method. It is verified that the numerical results do not depend on the discretization of the time or the momentum space.

### A. Classical vs quantum excitation

We first discuss the situation where we excite the semiconductor ground state, $|G\rangle$, with a classical light pulse that is resonant with the $1s$-exciton state. Figure 1(a) shows the optical pulse (shaded area), the induced optical polarization $|P|^2=|(1/\mathcal{V})\Sigma_{\mathbf{k}}P_{\mathbf{k}}|^2$ (dashed line), and the resulting density of optically active $1s$ excitons (dotted line). We note that $|P|^2$ increases and then decays exponentially with a rate of 2.6 ps where the polarization is converted dominantly into $1s$-exciton population. Due to the polarization-to-population conversion process via phonon and Coulomb scattering, the center-of mass distribution of the generated excitons, $\Delta N_{1s}(\mathbf{q})$, is rather broad [solid line in Fig. 1(b)]. Since only the low-momentum excitons are directly coupled to the light, the radiative recombination leads to a spectrally selective depletion (hole burning) of bright excitons while a majority of dark, large-momentum excitons remain in the system. Thus, the overall exciton population is only weakly coupled to the light field.

To obtain an interpretation of the classical excitation scenario, we remember that the coherent state [19,33] of light can be written as $|\beta\rangle=e^{\beta B^\dagger-\beta^\star B}|0\rangle\equiv D(\beta)|0\rangle$ with $\beta=\langle B\rangle$ according to Eq. (10). If we ignore for the moment all quasiparticle scattering processes, the coherent light excites the state $\hat{\rho}_S=D_X|G\rangle\langle G|D_X^\dagger$ [25,37] as shown also in Appendix D 1. Since $|G\rangle$ corresponds to vacuum $|0\rangle$ and $D_X$ is equivalent to $D(\beta)$ where $B$ is replaced by the $1s$-exciton operator $X_{1s}$,

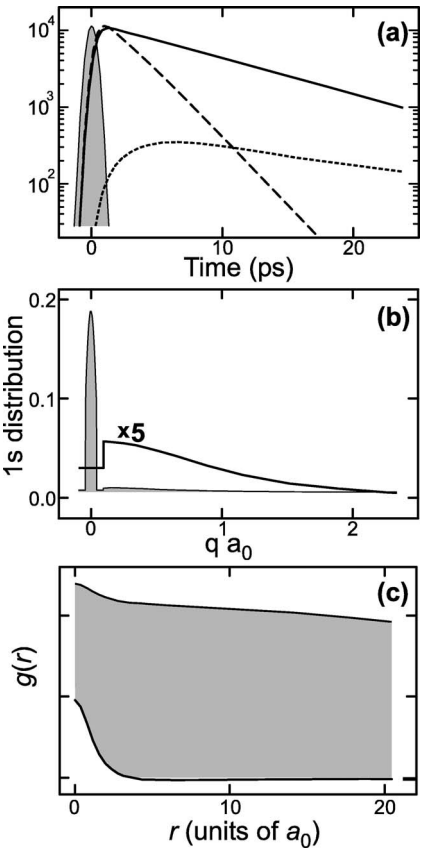


FIG. 1. Comparison of the excitation dynamics resulting from excitation with pulsed quantum and classical pump light. (a) The optical excitation pulse (arb. units) is shown as shaded area. Assuming classical light, this excitation generates optical polarization (dashed line, arb. units) $|P|^2$ which is partly converted into a population of $1s$ excitons (dotted line, $\mathrm{cm}^{-1}$) with the optical cone. Quantum excitation directly generates density of optically active $1s$ excitons (solid line, $\mathrm{cm}^{-1}$). (b) The distribution of excitons, $\Delta N_{1s}(q)$, resulting from quantum (dark area) and classical excitation (solid line, multiplied by 5) is plotted at 11 ps after the pulse maximum. (c) The pair-correlation function corresponding to the situation in (b) is shown as function of electron-hole pair distance $r$.

we realize that the optically induced quasiparticle state $\hat{\rho}_S$ has the same formal statistics as the exciting light. At the same time, $\hat{\rho}_S$ represents an interband polarization where each single carrier is in a coherent superposition state of conduction and valence bands. This excited state can also be described via a Gross-Pitaevski-type equation [41]—an approach famous in BCS theory and atomic condensates. However, a resonant excitonic polarization should not be confused with exciton particle condensation since scattering processes are needed to convert $P$ into a population which then exhibits a nondegenerate $\Delta N_{1s}(\mathbf{q})$ as shown in Fig. 1(b).

An example for a quantum excitation is shown in Fig. 1(a) where we assumed an excitation pulse (shaded area) with thermal quantum statistics but otherwise the same properties as the classical pulse. The generated density of optically active $1s$ excitons is plotted as solid line. Its dynamics reveals a striking phenomenon; the quantum excitation completely bypasses the polarization-to-population conversion

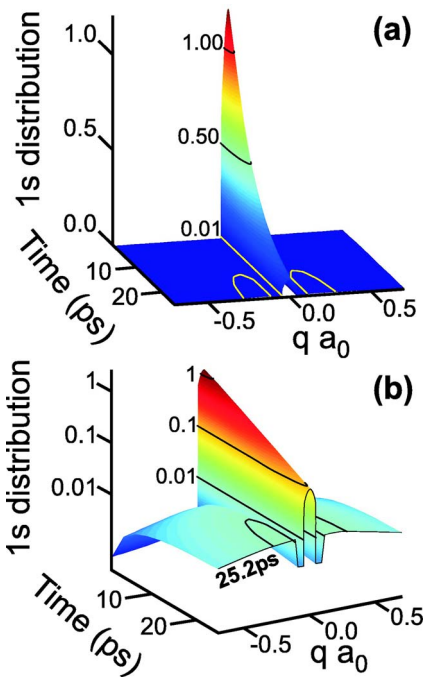


FIG. 2. (Color online) Computed dynamics of the exciton condensate after pulsed quantum excitation used in Fig. 1. (a) The evolution of the $1s$-exciton distribution $\Delta N_{1s}(\mathbf{q})$ is shown as a function of time. (b) Same data presented on a semilogarithmic scale.

by directly generating an exciton population—it is the inverse of spontaneous emission that converts light to population. The corresponding $\Delta N_{1s}(\mathbf{q})$ is now almost singular [dark area in Fig. 1(b)] indicating a macroscopic occupation of the lowest-momentum state. Figure 1(c) shows the corresponding pair-correlation function $g(\mathbf{r})$ indicating that the quantum excitation (dark area) leads to long-range order while classical excitation (solid line) does not. Hence, the thermal quantum excitation generates a quantum-degenerate exciton state, i.e., an exciton condensate. These observations verify the analytical predictions obtained in Sec. IV B.

The condensate in Fig. 1 is directly coupled to the light field such that the entire population recombines radiatively, here with a 10 ps decay constant which is a typical value for a single GaAs-type quantum well [4]. The interesting next question is to follow how the exciton distribution behaves as it decays radiatively. More precisely, Fig. 2(a) shows a sequence of exciton distributions for the quantum excitation used in Fig. 1; the same data are presented on a semilogarithmic scale in Fig. 2(b). We observe that the generated distribution remains ultranarrow and only a small tail develops toward high-momentum states. Thus, the exciton state remains degenerate throughout its radiative decay indicating that the exciton condensate experiences an anomalous reduction of Coulomb and phonon scattering. This observation actually validates the starting point of our analytic investigations, i.e., the assumption that scattering can be omitted to understand what kind of quasiparticle excitation is created by the quantum-excitation scheme. In addition, the semilogarithmic presentation of distributions nicely identifies that excitons, having momentum below $|qa_0|=0.047$, belong to the condensate generated by the quantum excitation with the 45° angular resolution. The remaining bright excitons are found with $0.047 \leqslant |qa_0| \leqslant 0.094$ corresponding to remaining angles 45°–90° in the optical cone. Both condensate and remaining bright excitons decay radiatively while the rest of the excitons with higher momenta are optically dark.

Because of the reduced interaction, we may investigate the basic properties of the quantum excitation by omitting the Coulomb and phonon scattering. With this simplification, the derivation in Appendix D 2 shows that thermal quantum light generates a state with $\langle [X_{1s}^{\dagger}]^J X_{1s}^K \rangle = \delta_{J,K} J! \Delta \langle X_{1s}^{\dagger} X_{1s} \rangle^J + \mathcal{O}(na_0)$ corresponding to a thermal state for sufficiently dilute density $n$. Again, the quantum statistics of the exciting light and the degenerate exciton states match. Furthermore, $\Delta N_{1s}(\mathbf{q})$ becomes a strict $\delta$ function as the angular spread of the quantum excitation approaches 0°. For example, two orders of magnitude higher and narrower $\Delta N_{1s}$ is reached by simply using a 0.45° angular resolution instead of the 45° angular resolution as in Figs. 1 and 2.

### B. Directionality of quantum emission

In addition to the macroscopic exciton population and anomalous reduction of scattering, one may anticipate that the exciton condensate exhibits an unusual quantum emission. For this purpose, we follow

$$I_{\mathrm{PL}}(\mathbf{q}) = \sum_{q_\perp} \frac{\partial}{\partial t} \Delta \langle B_{\mathbf{q},q_\perp}^{\dagger} B_{\mathbf{q},q_\perp} \rangle, \tag{44}$$

which defines the total flux of photons emitted into the direction $\mathbf{q}$. Experimentally, we suggest that the exciton condensate can be observed most strikingly via the extreme directionality of the quantum emission.

Figure 3(a) presents the luminescence into the direction allowed for the condensate emission (solid line) and into the remaining bright direction (hatched area). Here, we assumed pulsed quantum excitation corresponding to Figs. 1 and 2. As a comparison, the dashed line shows the photoluminescence after the coherent excitation used in Fig. 1. In this case, all emission directions are basically identical without preferred directionality. To quantify the level of degeneracy, we have also plotted the time evolution for the occupations of the exciton condensate (solid line), the bright excitons (hatched area), and the dark excitons (dark area) in Fig. 3(b). We observe that the emission from the condensate is more than two orders of magnitude larger than that in any other direction. This same factor is found for populations where the peak value of the exciton condensate is more than two orders of magnitude higher than that of the other states, in agreement with the analytic results for the generation of the exciton condensate. Thus, the strongly directional quantum emission stems directly from the highly singular exciton distributions. We also notice that both the exciton condensate and bright excitons decay radiatively. At the same time, the dark exciton populations increase very slowly, mainly due to phonon-induced scattering processes. Thus, the exciton distribution remains more or less singular during its decay dynamics.

In addition, we observe that the quantum excitation leads to orders of magnitude stronger quantum emission as com-

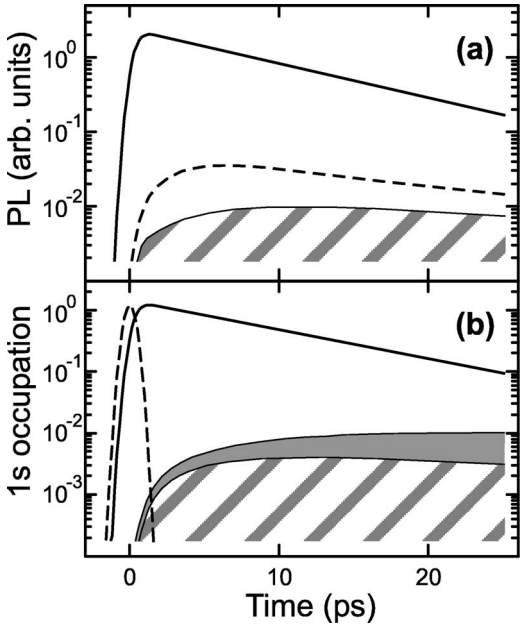


FIG. 3. Quantum emission after pulsed quantum excitation used in Fig. 1. (a) The evolution of the total luminescence is presented by plotting $I_{\mathrm{PL}}(q)$ into the direction allowed for the condensate (solid line) and the remaining bright excitons (hatched area). For comparison, we also show the total luminescence resulting from the classical excitation in Fig. 1 as a dashed line. (b) The corresponding occupations are plotted for the exciton condensate with $\Delta N_{1s}(0)$ (solid line), the remaining bright excitons with $\Delta N_{1s}(0.08)$ (hatched area), and the dark excitons (dark area) with $\Delta N_{1s}(0.2)$. The temporal dynamics of the quantum pump is displayed as the dashed line.

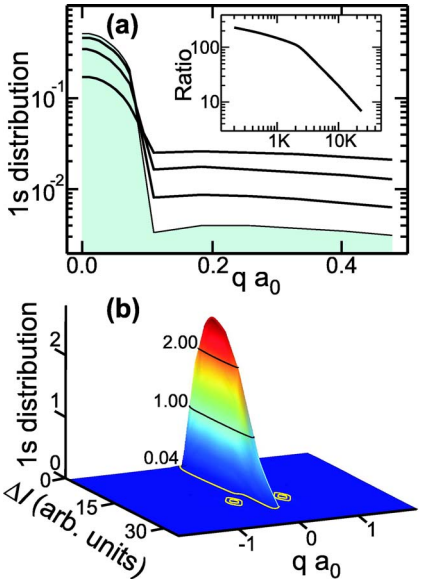


FIG. 4. (Color online) Stability of the exciton condensate after quantum excitation. (a) The computed $\Delta N_{1s}(q)$ is plotted 11 ps after the pulse maximum (see Fig. 1); the lattice temperature changes from 1 to 24 K (bottom to top) and the inset shows the ratio $\Delta N_{1s}(0)/\Delta N_{1s}(0.2)$. (b) Distribution $\Delta N_{1s}(q)$ is shown as a function of intensity of quantum excitation.

pared with the classical excitation situation. Due to its strongly enhanced quantum emission, it is clear that photoluminescence from the seeded exciton condensate can be detected even for orders of magnitude lower excitation levels compared with ordinary classical or nonresonant excitation schemes. It is interesting to notice that the enhanced coupling of the exciton condensate to the light field also means faster radiative decay of quasiparticle excitations than that observed after classical or nonresonant excitations. After quantum excitation, the entire excitation decays with the radiative decay constant of the condensate which was observed to be roughly 10 ps for the conditions studied in Fig. 1. Consequently, the excitation vanishes in some tens of picoseconds. In comparison to this, classical light generates quasiparticle excitations that remain in the system typically for nanoseconds due to the strongly reduced coupling of the quasiparticles to the light field.

### C. Stability of exciton condensate

We test the stability of the seeded exciton condensate by evaluating $\Delta N_{1s}(\mathbf{q})$ as function of the lattice temperature $T$ [Fig. 4(a)] and the excitation intensity $\Delta I \equiv \Delta\langle B^{\dagger}B\rangle$ at 4 K [Fig. 4(b)]. In both cases, the degenerate state is remarkably stable against increased scattering. To have a clearer analysis, we use the full optical cone ($0°-90°$) in the excitation and assume $\frac{1}{10}$ reduction of the radiative coupling compared with Fig. 1. The inset to Fig. 4(a) quantifies the level of phonon scattering by showing the ratio of the low-momentum and high-momentum populations as function of $T$. Strongly singular $\Delta N_{1s}$ is observed for all used $T$ while phonon scattering becomes orders of magnitude weaker as $T \to 0$. In Fig. 4(b), the macroscopic population of the $1s$ state continuously increases up to the intensity level $\Delta I = 10$ which corresponds to the generated carrier density $na_0 = 0.1$. For higher excitation levels, the $1s$-exciton population starts to decrease because the underlying fermion character of the electron-hole pairs gradually prevents further exciton accumulation. The quantum-degenerate state ceases to exist above $\Delta I = 31$ with $na_0 = 0.3$.

Figure 4(b) gives an overview of our calculations for pulsed quantum excitations. The generation of the exciton condensate becomes less efficient as a carrier density is reached where $na_0 = 0.1$. In other words, the macroscopic population is reduced even though the intensity of the excitation is increased. This phenomenon originates from the fermionic blocking and scattering effects omitted in the analytic investigations. It is intuitively clear that it is more difficult to generate the exciton condensate if this requires us to put two or more similar fermions close to each other. The number $na_0 = 0.1$ estimates that one observes on average 0.1 similar fermions within the radius of a bound electron-hole pair. According to our calculations, this seems to be the limit indicating elevated fermion and scattering effects for the condensate.

Since our theory can also be applied for the cases where one mixes quantum and classical excitation schemes, we may now investigate whether the observed quantum effects are stable against the level of classical components in the

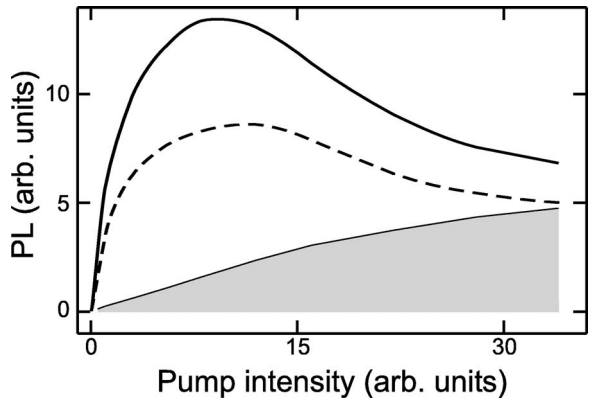


FIG. 5. Computed total photoluminescence $I_{PL}(0)$ in the direction allowed for the condensate resulting from a mixture of pulsed classical and quantum excitations. The excitations have the same temporal dynamics as in Fig. 1 and the luminescence is determined 16 ps after the pulse maximum. Full quantum excitation (solid line) is compared with 40% coherent (dashed line) and 100% coherent, i.e., fully classical, (shaded area) excitations.

pump source. As an example, we show in Fig. 5 the total luminescence as function of pump intensity determined 16 ps after pure quantum excitation, i.e., 0% coherent part (solid line), mixed excitation with 40% coherent part (dashed line), and fully classical excitation with 100% coherent part (shaded area). To have a one-to-one comparison, we use the same temporal and spectral pump pulses as in Fig. 1. We see that for the relatively low levels of excitation studied here, the total luminescence for the 100% coherent case exhibits the expected practically linear dependence on the excitation strength. However, when we include an incoherent quantum component to the excitation process, $I_{PL}$ behaves nonmonotonically. Even more so, for weak to moderate intensities, the quantum excitation scheme leads to light emission that is enhanced by orders of magnitude in comparison to that of classical excitation.

If we now return to the quantitative analysis, we observe that the luminescence is maximized at the intensity level $\Delta I=10$ corresponding to the maximum singularity of exciton distributions in Fig. 4(b) for 100% incoherent quantum excitation. Since the population of the zero-momentum state decreases for elevated intensities, the luminescence decreases also until it reaches the same level as that for coherent excitation. This predicted, distinctively nonmonotonic, behavior of $I_{PL}$ should be directly observable in experiments serving as a clear signature for the formation of the quantum-degenerate exciton state. We note in Fig. 5 that $I_{PL}$ has a maximum even in the presence of 40% coherent excitation, indicating that an appreciable population in the quantum-degenerate state is generated even in this imperfect case.

### D. Quantum excitation with quasi-cw source

For the experimental realization of quantum-optical spectroscopy, one needs well-characterized sources of thermal light which can be realized by using spectrally narrow spontaneous emission of other systems. There is also the theoretical prediction [42] of how to generate incoherent pulses by

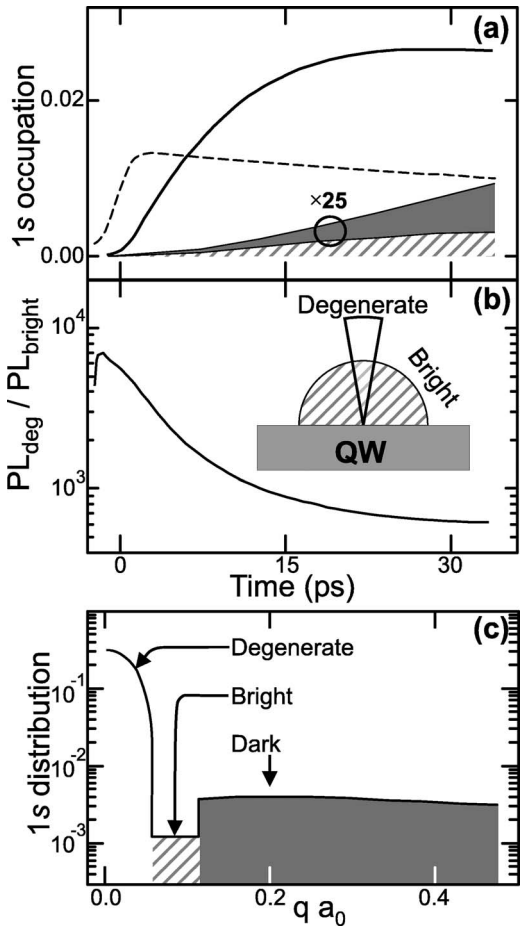


FIG. 6. The exciton condensate induced by quasi-cw quantum excitation. (a) Incoherent quantum excitation (dashed line, scaled) predominantly generates a degenerate 1$s$-exciton occupation (light area); the residual bright (hatched area), and dark (dark area) occupations are multiplied by 25. (b) The directionality of quantum emission is studied by plotting the ratio of the luminescence from the degenerate and the other bright exciton states. The directionality of the emission (schematic inset) is determined by the angular resolution of the pump. (c) The computed $\Delta N_{1s}(q)$ 34 ps after the onset of excitation.

controlling spontaneous emission coherently. After spectral, temporal, and directional diagnostics of incoherent quantum emission have been implemented, one may also ask how to detect quantum-degenerate exciton states. Here, we think that the conceptually simplest measurement would be to monitor the directionality of the quantum emission, i.e., photoluminescence. While a conventional exciton and/or electron-hole-pair distribution emits into all directions, the condensate emission is highly directional.

Since it may be experimentally challenging to obtain temporally short incoherent light pulses, we also study excitation with a long incoherent, i.e., a quasi-continuous-wave source with thermal statistics. By using such an excitation, 45° angular resolution, and 1 K lattice temperature, one generates the exciton occupation $\Delta N_{1s}(q)$ shown in Fig. 6(a) for degenerate ($q=0$, solid line), bright ($qa_0=0.08$, hatched area), and dark ($qa_0=0.2$, dark area) excitons. We see that the degenerate and bright $\Delta N_{1s}$ saturate toward a steady state due to

radiative decay while the occupation of dark exciton states continues to rise linearly mainly due to phonon scattering. The complete range of $\Delta N_{1s}(q)$ is shown in Fig. 6(c) at $t=34$ ps. We observe a strongly peaked, degenerate exciton state, hole burning for bright nondegenerate excitons, and tailing of dark excitons beyond the optical cone ($0°-90°$). For the conditions assumed in this calculation, the populations in dark states reach the level of the degenerate state after approximately 2 ns. However, this time can be made considerably longer with a narrower angular resolution making the exciton condensate observable via presently available incoherent light sources.

Directional quantum emission is analyzed in Fig. 6(b) via the ratio of photoluminescence into the degenerate ($0°-45°$) vs remaining bright direction ($45°-90°$) resulting from the excitation in Fig. 6(a). After the initial transients ($<0$ ps), the quantum emission into the degenerate direction becomes almost three orders of magnitude stronger than in other directions. In comparison, the quantum emission after classical excitation is not directional and its intensity is very small compared with the quantum excitation case as shown in Fig. 3(a) for pulsed excitations. Thus, photoluminescence of a degenerate state can be monitored with much lower excitation levels compared with excitonic luminescence resulting from electron-hole plasma or nondegenerate exciton distributions [43].

To complete this investigation, we also performed the analysis for quasi-cw quantum excitation by increasing its intensity. Figure 7 presents the quantum emission from the condensate into the degenerate direction (solid line) and emission by bright excitons in all other directions (hatched line) as function of quasi-cw pump intensity; see also inset to Fig. 6(b) for a schematic distinction of these directions. The same data are presented on a linear scale in Fig. 7(a) and on a double-logarithmic scale in Fig. 7(b). We observe that the exciton condensate displays a nonmonotonic dependence on the quasi-cw pump intensity whereas the remaining bright excitons exhibit a linear intensity dependence. The maximum condensate emission is obtained at the intensity $\Delta I=30$ while the emission becomes nearly nondirectional at $\Delta I=90$. As other general trends we observe that (i) the emission into the bright direction grows linearly for almost all intensities and (ii) it is more than two orders of magnitude lower than the condensate emission.

Figure 8 shows the generated exciton distributions as function of excitation intensity $\Delta I$; the distribution is evaluated 25 ps after the switch on of the quasi-cw quantum excitation corresponding to Fig. 6(a). We observe that the population of the exciton condensate increases up to $\Delta I=30$ corresponding to the carrier density $na_0=0.1$. As the excitation level is increased further, the condensate becomes less pronounced and it vanishes completely at $\Delta I=90$ corresponding to $na_0=0.25$. These intensity values are synchronized with those leading to the maximum condensate emission and the loss of directionality in Fig. 7. Thus, we observe that the luminescence maximum and the peak value of the condensate occupation are directly related such that the overall nonlinear behavior of the luminescence stems from the interplay between buildup of a condensate and its eventual

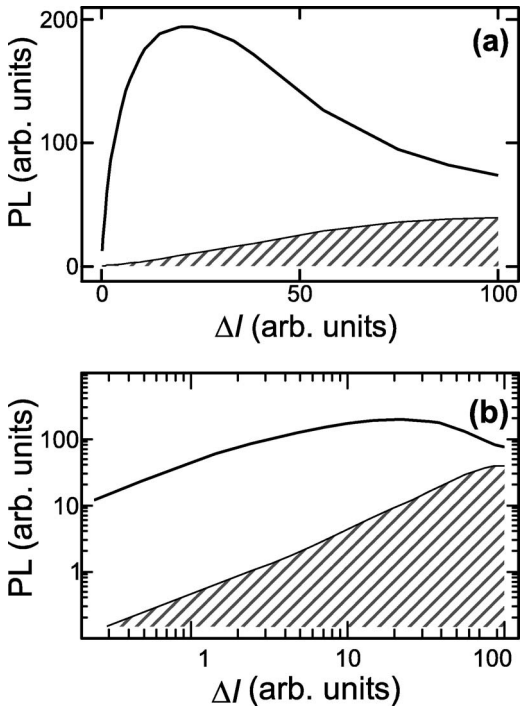


FIG. 7. Quantum emission for quasi-cw excitation. The computed luminescence intensity (at 25 ps after the onset of excitation) of the condensate (solid line) is compared with the emission of the other optically active excitons (hatched area) for different excitation intensities in (a) linear and (b) double-logarithmic scale. The numerical parameters are the same as in Fig. 6.

destruction by fermionic scattering and blocking effects (see also Figs. 4 and 5). In addition, the limiting densities are very similar to those obtained for the pulsed excitation in Fig. 4 showing that the fermionic phase-space filling and scattering effects are rather insensitive to the way the exciton condensate is generated.

To explore the fermionic effects in more detail, we also show the $1s$-exciton occupations in the condensate (solid line), in the remaining bright states (hatched area), and in

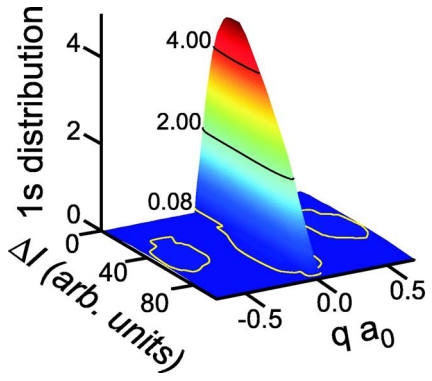


FIG. 8. (Color online) Stability of the exciton condensate for varying intensity of the quasi-cw quantum pump used in Figs. 6 and 7. The computed $1s$ distribution $\Delta N_{1s}(q)$ is shown as a function of exciton momentum and excitation intensity $\Delta I$. Distributions are evaluated numerically at 25.2 ps after the switch on of the excitation (see Fig. 6 for a typical evaluation).

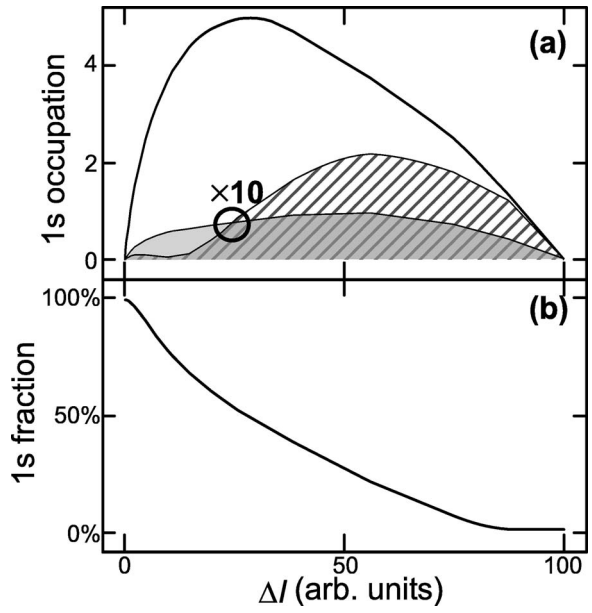


FIG. 9. Stability of the exciton condensate for varying intensity of the quasi-cw-quantum pump used in Figs. 6–8; all quantities are evaluated numerically at 25.2 ps after the switch on of the excitation. (a) The occupations are shown for the exciton condensate with $\Delta N_{1s}(0)$ (solid line), the remaining bright excitons with $\Delta N_{1s}(0.08)$ (hatched area, multiplied by 10), and the dark excitons with $\Delta N_{1s}(0.2)$ (dark area, multiplied by 10). (b) The corresponding total fraction of $1s$ excitons, $\Delta n_{1s}/n$, with respect to total electron-hole density $n$ is shown.

dark states (dark area) in Fig. 9(a) as function of excitation intensity. The corresponding total $1s$-exciton fraction $X_{1s}=\Sigma_q \Delta N_{1s}(q)/\Sigma_k f_k^e$ with respect to the generated carrier density $n=(1/\mathcal{L})\Sigma_k f_k^e$ is plotted in Fig. 9(b). We observe now that the generation of $1s$ excitons stops at the intensity $\Delta I=90$ because of exciton ionization, as discussed above. This is further supported by the fact that the quantum emission loses its directionality around this intensity (see Fig. 7). However, we find that the macroscopic occupation remains orders of magnitude larger than that of other exciton states almost up to the ionization threshold. This once again underlines the robustness of the condensate due to the anomalous reduction in scattering.

In general, the results of our computations presented in Figs. 1–9 show that quantum-optical spectroscopy leads to intriguing effects due to the quantum-degenerate exciton state. Testing parameter variations, we find that the predicted phenomena can be observed as long as the excitation is dominantly (>50%) quantum, lattice temperatures are below roughly 20 K, and electron density is less than about 0.2 particles within the exciton Bohr radius. In practice, one might use photoluminescence from other similar systems as a quantum source, temperatures below 20 K are standard in cryogenic experiments, and the limiting densities are reachable (e.g., typical GaAs parameters give a density estimate $2\times10^5$ cm$^{-1}$ in quantum wires and $4\times10^{10}$ cm$^{-2}$ in quantum wells for the upper-limit density where the exciton condensate can still be present) and the corresponding emission is detectable in current experiments [40,43]. Thus, we believe that experiments on quantum-optical spectroscopy can be realized in high-quality semiconductor samples along the lines presented in this paper.

## VI. GENERAL PRINCIPLE OF QUANTUM-OPTICAL SPECTROSCOPY

Our results show that both classical and quantum excitation induce quasiparticle states whose statistical properties are close to those of the exciting light. In particular, a resonant classical excitation generates a coherent excitonic polarization which then decays to other states, whereby its coherent features are rapidly erased as seen in Fig. 1. In contrast to this, quantum excitation generates a degenerate exciton state, i.e., a condensate. In this connection, several spectacular features were found related to the state, its interactions, and quantum-optical emission. These observations can be summarized altogether as the *general principle of quantum-optical spectroscopy* for direct-gap semiconductors: (i) light seeds a quantum-degenerate quasiparticle state with nearly identical quantum statistics as that of the light; (ii) the quantum statistics of the degenerate state determines how it interacts with other quasiparticles and states; and (iii) the properties of the state and its subsequent evolution show up in the quantum emission.

In atomic systems, quantum-degenerate states have been successfully realized via Bose-Einstein condensation [44–47]. Several impressive features like interference effects, long-range order, and entanglement effects have been observed [48,49]. As an even more intriguing feature, the degenerate state is internally an infinite-dimensional quantum object spanned by the number states of a harmonic oscillator. As our investigations show, exactly this quantum-statistical extension controls the character of interactions between the degenerate and other states or systems. In atomic condensates, the connection of interactions and quantum statistics of number, squeezed, and coherent state states has already been experimentally established [50]. The dependency of interactions on the quantum statistics is actually a general feature since, e.g., analogous quantum-state-dependent quantum-Rabi oscillations have been predicted [51] and observed [52] between cavity photons and an atom. Since semiconductors inherently are strongly interacting systems, one would ultimately like to use a variety of degenerate states to explore and control the many-body interaction effects in solids via the different forms of quantum states they can be excited into.

For this purpose, we consider the quantum statistics of a generic bosonic state—which can describe either the quantized light field or a degenerate semiconductor state at low densities—defined by creation, $b^\dagger$, and annihilation, $b$, operators. Then the quantum statistics follows from the normally ordered $(J+K)$-particle expectation values

$$I_K^J \equiv \langle [b^\dagger]^J b^K \rangle = (-1)^K \frac{\partial^J}{\partial \eta^J} \frac{\partial^K}{\partial \eta^{\star K}} \chi(\eta, \eta^\star)\Big|_{\eta=0}, \tag{45}$$

$$\chi(\eta,\eta^\star)=\sum_{J,K=0}^{\infty}\frac{(-1)^K}{J!\,K!}I_K^J\eta^J[\eta^\star]^K,$$

which also defines the characteristic function $\chi(\eta,\eta^\star)$. The Taylor expansion between $I_K^J$ and $\chi(\eta,\eta^\star)$ shows that they are uniquely connected when $\chi(\eta,\eta^\star)$ is an analytic function, as it is for physical states.

The cluster expansion can also be applied to the quantum-degenerate state, yielding

$$\chi(\eta,\eta^\star)\equiv e^{\xi(\eta,\eta^\star)},$$
$$\xi(\eta,\eta^\star)=\ln[\chi(\eta,\eta^\star)]=\sum_{J,K=0}^{\infty}\frac{(-1)^K}{J!\,K!}\Delta I_K^J\eta^J\eta^{\star K}, \tag{46}$$

where $\Delta I_K^J$ corresponds to correlated $(J+K)$-particle clusters. At the same time, this is a generalization of cumulants [53] of statistical distributions; see also Ref. [54] where cumulants of number distributions are derived for an atomic condensate. This allows us to generalize the principle of quantum-optical spectroscopy beyond the examples presented in this paper since $\Delta I_K^J$ of the light field and $(J+K)$-particle correlations of the matter are directly coupled within the same class of correlation equations whereas coupling to other classes takes place via higher-order effects like scattering. This conclusion follows from the light-matter interaction $H_D$ in Eq. (2) and how it appears in the hierarchy problem (5) as the cluster-expansion identification (6) is performed. Thus, the $\Delta I_K^J$ correlation of light drives and seeds a degenerate quasiparticle state in the semiconductor with nearly identical correlations. Since the nature of subsequent scattering dynamics is strongly influenced by the seeded quantum statistics and the realized excitation level, the general quantum-optical spectroscopy should be a versatile method to chart further quasiparticle excitations as well as to enhance, suppress, and control interactions in semiconductor many-body systems.

We now classify the different possibilities to apply quantum-optical spectroscopy at the level of two-particle correlations in Eq. (46). In this case, $\chi(\eta,\eta^\star)$ contains only correlations up to $(J+K)\leqslant 2$. The corresponding density matrix can be worked out:

$$\hat\rho_{SD}=D(\beta)S(\xi)\hat\rho_{\rm th}(n_{\rm th})S^\dagger(\xi)D^\dagger(\beta),\quad S(\xi)\equiv e^{(\xi^{\star 2}B^2-\xi^2B^{\dagger 2})/2}, \tag{47}$$

where we recognize the displacement operator $D(\beta)$ described in the classical excitation scheme, the thermal state $\hat\rho_{\rm th}$ used for the quantum excitation, and then a squeezing operator $S(\xi)$ which leads to a more general quantum excitation. Thus, the singlet-doublet level already includes the central concepts used in quantum-optics theory [19,33].

In general, the parameters $\beta$, $\xi$, and $n_{\rm th}$ classify the quantum-optical spectroscopy performed at the level of two-particle correlations. They have a simple form after we define canonical quadrature operators $x=(B+B^\dagger)/2$ and $y=(B-B^\dagger)/2i$ and their maximum and minimum fluctuations,

$$\Delta x\equiv[\langle xx\rangle-\langle x\rangle\langle x\rangle]^{1/2}_{\rm max}=\tfrac{1}{2}\sqrt{1+2\Delta\langle B^\dagger B\rangle+2|\Delta\langle BB\rangle|},$$
$$\Delta y\equiv\tfrac{1}{2}\sqrt{1+2\Delta\langle B^\dagger B\rangle-2|\Delta\langle BB\rangle|}, \tag{48}$$

respectively. Since $x$ and $y$ are a canonical pair, the fluctuations must obey the Heisenberg uncertainty principle

$$\Delta x\Delta y\geqslant\tfrac{1}{4}. \tag{49}$$

With help of these, one finds

$$\beta=\langle B\rangle,\quad n_{\rm th}=2\left(\Delta x\Delta y-\frac{1}{4}\right),\quad \xi=\frac{q}{|q|}\ln\frac{\Delta y}{\Delta x}. \tag{50}$$

In this form, we see that $\langle B\rangle$ defines the coherent—classical—displacement, $n_{\rm th}$ tells us how much the quantum fluctuations exceed the Heisenberg minimum-uncertainty limit equal to $\frac{1}{4}$, while $\xi$ shows how much quadrature fluctuation in $y$ are squeezed with respect to those in quadrature $x$. In our quantum excitation, we did not apply squeezed states since squeezed sources are much more difficult to realize experimentally than thermal sources.

## VII. SUMMARY

In summary, our results promote the general principle of quantum-optical spectroscopy where the statistical properties of the exciting light strongly influence the nature of the generated quasiparticle state. We use the example of direct-gap semiconductors to identify excitation conditions that induce quantum states whose statistical properties differ drastically from those of classically generated states. The calculations show that experimentally feasible quantum light sources can seed an exciton condensate which has a nearly singular momentum distribution leading to anomalously reduced Coulomb and phonon scattering. The quantum emission from that state is strongly enhanced, highly directional, and shows an unusual nonmonotonic intensity dependence. These observations should encourage the expansion of optical spectroscopy to a direction where both the exciting pulses and the emission are controlled and diagnosed at the quantum-statistical level.

The possibility of squeezing as well as other new classes of quantum sources lead to schemes which are able to excite different types of degenerate quasiparticle states. As a generalization of the examples shown so far, one can think of using more complicated quantum fields yielding degenerate quasiparticle states with higher-order correlations. The subsequent quantum emission could then be used to gain information on how those correlations are modified and eventually decay due to the many-body interactions. In this context, a truly quantum-optical experiment should aim to control, measure, and diagnose the quantum statistics of both the exciting source and the light emission from the semiconductor. Based on our results, one can anticipate that such measurements not only should access a multitude of quantum-optical phenomena but should also provide extraordinary and superior schemes to measure and control various many-body effects in semiconductors in comparison to similar classical spectroscopy. Thus, we expect that quantum-optical spectros-

copy will reshape the level of understanding and applicability of semiconductors as true quantum devices.

## ACKNOWLEDGMENTS

This work was supported by the Deutsche Forschungsgemeinschaft through the Quantum Optics in Semiconductors Research Group and by the Optodynamics Center of the Philipps-Universität Marburg.

## APPENDIX A: FORMAL ASPECTS OF THREE-PARTICLE SCATTERING TERMS

In this Appendix, we present aspects of the formal cluster-expansion truncation (7) up to the level of triplets. Specifically, we show how the three-particle scattering terms are obtained. We start from Eq. (5) and include only terms up to three-particle correlations, which leads to the general equation structure

$$i\hbar\frac{\partial}{\partial t}\langle 1\rangle = T_1[\langle 1\rangle] + V_1[\langle 2\rangle_S] + V_1[\Delta\langle 2\rangle], \tag{A1}$$

$$i\hbar\frac{\partial}{\partial t}\Delta\langle 2\rangle = T_2[\Delta\langle 2\rangle] + V_{2a}[\langle 3\rangle_{\mathrm{SD}}] + V_{2b}[\Delta\langle 3\rangle], \tag{A2}$$

$$i\hbar\frac{\partial}{\partial t}\Delta\langle 3\rangle = T_3[\Delta\langle 3\rangle] + V_3[\langle 4\rangle_{\mathrm{SDT}}], \tag{A3}$$

where $T_{1(2,3)}$ and $V_{1(2,3)}$ are known functionals defined by the specific form of the corresponding Heisenberg equations of motion. Consequently, the hierarchy is systematically truncated resulting in a finite number of coupled equations.

The full singlet-doublet-triplet structure (A1)–(A3) is still beyond the current numerical capabilities if one wants to study quantum-well or quantum-wire systems numerically. However, one can find a clear physical way to simplify the triplet dynamics (A3) since it contains two distinct classes of effects: (i) the simpler microscopic processes describe the scattering of two-particle correlations from single-particle quantities while (ii) the more complicated terms are responsible for the formation of genuine three-particle correlations like trions. For example, the first class implies that an exciton can scatter with an electron, hole, or phonon, which leads to screening of the Coulomb interaction, dephasing of coherences, and formation or equilibration of excitons [28–30]. Since the formation of trions is slow after optical excitations and requires high densities beyond the exciton Mott transition to become relevant [31,32], we omit genuine three-particle correlations from the analysis. This considerably simplifies the numerical effort and we end up with a consistent singlet-doublet approach which includes electrons, holes, excitons, and scattering among them as well as the most important quantum-optical effects at the same fundamental level.

The structure of the corresponding numerically feasible triplet equations follows from

$$i\hbar\frac{\partial}{\partial t}\Delta\langle 3\rangle = T_3[\Delta\langle 3\rangle] + V_3[\langle 4\rangle_{\mathrm{SD}}], \tag{A4}$$

where the four-particle terms are factorized up to two-particle terms. The simpler functional $T_3$ can be written in the form $T_3[\Delta\langle 3\rangle]=(\Delta E-i\gamma)\Delta\langle 3\rangle$ where $\Delta E$ is the energy difference of the in- and out-scattering for single-particle terms and two-particle correlations. Based on the approximation to omit genuine three-particle correlations, $V_3[\langle 4\rangle_{\mathrm{SD}}]$ does not contain triplets in contrast to the full Eq. (A3). Thus, $\Delta\langle 3\rangle$ can be solved analytically,

$$\Delta\langle 3\rangle = \frac{1}{i\hbar}\int_{-\infty}^{t} V_3[\langle 4\rangle_{\mathrm{SD}}](u)e^{i(\Delta E-i\gamma)(u-t)/\hbar}du. \tag{A5}$$

As a general feature, the microscopic scattering effects in semiconductors display non-Markovian characteristics that are relevant mostly at femtosecond time scales. Since we are interested in two-to-three orders of magnitude longer time scales, Eq. (A5) can be solved using the Markov approximation leading to

$$\Delta\langle 3\rangle = -\frac{V_3[\langle 4\rangle_{\mathrm{SD}}](t)}{\Delta E - i\gamma}. \tag{A6}$$

Inserting this solution into Eq. (A2), we find

$$i\hbar\frac{\partial}{\partial t}\langle 1\rangle = T_1[\langle 1\rangle] + V_1[\langle 2\rangle_S] + V_1[\Delta\langle 2\rangle], \tag{A7}$$

$$i\hbar\frac{\partial}{\partial t}\Delta\langle 2\rangle = T_2[\Delta\langle 2\rangle] + V_{2a}[\langle 3\rangle_{\mathrm{SD}}] + G[\langle 1\rangle,\Delta\langle 2\rangle], \tag{A8}$$

where the functional $G[\langle 1\rangle,\Delta\langle 2\rangle]$ indicates that three-particle correlations are included at the scattering level. This fundamental form is the starting point of our quantum-optical investigations for semiconductors.

## APPENDIX B: THE QUANTUM-OPTICAL EXCITATION SCHEME IN THE EXCITON BASIS

In general, the precise solution of quantum-optical spectroscopy inevitably leads to a rather complicated set of nonlinear equations. However, it is often intuitively instructive to view the underlying physics by expanding into an exciton basis, which also establishes a convenient platform to perform approximations that can help us to understand how the full equations describe a given physical phenomenon. Such an approach is developed in this appendix.

Both Eq. (15) for the polarization and the exciton Eq. (22) have a homogeneous part which defines an eigenvalue problem

$$\tilde{\epsilon}_{\mathbf{k}}\phi_{\lambda}^{R}(\mathbf{k}) - (1-f_{\mathbf{k}}^{e}-f_{\mathbf{k}}^{h})\sum_{\mathbf{k}'} V_{\mathbf{k}-\mathbf{k}'}\phi_{\lambda}^{R}(\mathbf{k}') = E_{\lambda}\phi_{\lambda}^{R}(\mathbf{k}). \tag{B1}$$

In the low-density limit $f_{\mathbf{k}}^{e}=f_{\mathbf{k}}^{h}=0$, Eq. (B1) becomes mathematically equivalent to the Fourier-transformed hydrogen

problem. Thus, for low densities Eq. (B1) has bound states, i.e., exciton solutions [5]. For elevated densities, $f^e_{\mathbf{k}}$ and $f^h_{\mathbf{k}}$ are nonzero such that the problem becomes non-Hermitian. Consequently, Eq. (B1) has both left-handed, $\phi^L_\lambda(\mathbf{k})$, and right-handed, $\phi^R_\lambda(\mathbf{k})$, solutions connected and normalized via

$$\phi^L_\lambda(\mathbf{k}) = \frac{\phi^R_\lambda(\mathbf{k})}{1 - f^e_{\mathbf{k}} - f^h_{\mathbf{k}}}, \quad \sum_{\mathbf{k}} \phi^L_\lambda(\mathbf{k})\phi^R_\nu(\mathbf{k}) = \delta_{\lambda,\nu}, \tag{B2}$$

respectively. Since $\phi^{R/L}$ can be chosen to be a real-valued function, we implicitly apply this property in the following. Using the exciton wave functions we can transform the polarization into the exciton basis

$$p_\lambda = \sum_{\mathbf{k}} \phi^L_\lambda(\mathbf{k}) P_{\mathbf{k}}, \quad P_{\mathbf{k}} = \sum_{\lambda} p_\lambda \phi^R_\lambda(\mathbf{k}). \tag{B3}$$

For the two-particle exciton correlation, we use an analogous transformation,

$$\Delta\langle X^\dagger_{\lambda,\mathbf{q}} X_{\nu,\mathbf{q}}\rangle = \sum_{\mathbf{k},\mathbf{k}'} \phi^L_\lambda(\mathbf{k})\phi^L_\nu(\mathbf{k}') c_X^{\mathbf{q},\mathbf{k}'-\mathbf{q}_h,\mathbf{k}+\mathbf{q}_e},$$

$$c_X^{\mathbf{q},\mathbf{k}'-\mathbf{q}_h,\mathbf{k}+\mathbf{q}_e} = \sum_{\lambda,\nu} \phi^R_\lambda(\mathbf{k})\phi^R_\nu(\mathbf{k}')\Delta\langle X^\dagger_{\lambda,\mathbf{q}} X_{\nu,\mathbf{q}}\rangle, \tag{B4}$$

with $\mathbf{q}_e = [m_e/(m_e+m_h)]\mathbf{q}$ and $\mathbf{q}_h = [m_h/(m_e+m_h)]\mathbf{q}$. By applying Eq. (B3) in Eq. (15) and Eq. (B4) in Eq. (22), we obtain

$$i\hbar \frac{\partial}{\partial t} p_\lambda = E_\lambda p_\lambda - d_{vc}\phi^R_\lambda(\mathbf{r}=\mathbf{0})\langle E(t)\rangle - i\Gamma_\lambda, \tag{B5}$$

$$\begin{aligned} i\hbar \frac{\partial}{\partial t}\Delta\langle X^\dagger_{\lambda,\mathbf{q}} X_{\nu,\mathbf{q}}\rangle &= (E_\nu - E_\lambda)\Delta\langle X^\dagger_{\lambda,\mathbf{q}} X_{\nu,\mathbf{q}}\rangle \\ &\quad - (E_\nu - E_\lambda)\langle X^\dagger_{\lambda,\mathbf{q}} X_{\nu,\mathbf{q}}\rangle_S + iG^{\lambda,\nu}(\mathbf{q}) \\ &\quad + D^{\lambda,\nu}_{\mathrm{rest}}(\mathbf{q}) + T^{\lambda,\nu}(\mathbf{q}), \end{aligned} \tag{B6}$$

where $\phi^R_\lambda(\mathbf{r}=\mathbf{0}) \equiv \Sigma_{\mathbf{k}}\phi^R_\lambda(\mathbf{k})$. The singlet scattering $S^{\mathbf{q},\mathbf{k}',\mathbf{k}}$ in Eq. (22) leads to a source

$$\langle X^\dagger_{\lambda,\mathbf{q}} X_{\nu,\mathbf{q}}\rangle_S = \sum_{\mathbf{k}} \phi^L_\lambda(\mathbf{k}) f^e_{\mathbf{k}+\mathbf{q}_e} f^h_{\mathbf{k}-\mathbf{q}_h} \phi^L_\nu(\mathbf{k}). \tag{B7}$$

The other sources are expressed symbolically as $\Gamma_\lambda$, $G^{\lambda,\nu}(\mathbf{q})$, $D^{\lambda,\nu}_{\mathrm{rest}}(\mathbf{q})$, and $T^{\lambda,\nu}(\mathbf{q})$.

Even though Eqs. (B5)–(B7) have a seemingly simple form, the consistent solution is highly nontrivial since the two-particle correlations in $\Gamma_\lambda$, $G^{\lambda,\nu}(\mathbf{q})$, $D^{\lambda,\nu}_{\mathrm{rest}}(\mathbf{q})$, and $T^{\lambda,\nu}(\mathbf{q})$ contain truly fermionic contributions which do not have a simple form in the exciton basis. Thus, it is always advantageous to numerically evaluate the full problem in the original electron-hole picture. However, Eqs. (B3)–(B7) allow us to obtain the interesting excitonic quantities by projecting the results of the full computation into the exciton basis.

The features of quantum excitation can be elucidated by introducing an exciton basis. For simplicity, we assume that the excitation propagates in the perpendicular direction, i.e., $F(\mathbf{q}) = \mathcal{S}\delta_{\mathbf{q},0}$. As discussed in Sec. IV, we additionally assume that the back coupling of the photon-assisted polarization can be neglected.

We introduce the photon-assisted polarization in the exciton-basis representation via

$$\Pi_{\lambda,\mathbf{q},q_\perp} = \sum_{\mathbf{k}} \phi^L_\lambda(\mathbf{k})\Pi_{\mathbf{k},\mathbf{q},q_\perp}, \quad \Pi_{\mathbf{k},\mathbf{q},q_\perp} = \sum_{\lambda} \Pi_{\lambda,\mathbf{q},q_\perp}\phi^R_\lambda(\mathbf{k}). \tag{B8}$$

As for the classical excitation, the essence of quantum excitation can be analyzed by omitting the scattering processes. Thus, the exciton representation of Eq. (32) leads to

$$\begin{aligned} \frac{\partial}{\partial t}\Pi_{\lambda,\mathbf{q},q_\perp} &= i\left(\omega_{q_\perp} - \frac{1}{\hbar}E_{\lambda,\mathbf{q}}\right)\Pi_{\lambda,\mathbf{q},q_\perp} \\ &\quad - \delta_{\mathbf{q},0}\phi^R_\lambda(\mathbf{r}=\mathbf{0})\Delta\langle B^\dagger_{0,q_\perp} B_{0,\Sigma}\rangle - T^{\Pi}_{\lambda,0,q_\perp}, \end{aligned} \tag{B9}$$

where we have omitted the spontaneous emission source because the reemission from the generated carrier excitation is assumed to have a small influence on the generated state. From here we see that one dominantly generates the $1s$ component of $\Pi$ once the frequency of the quantum excitation coincides with the $1s$ resonance. Since the quantum excitation is present only for $\mathbf{q}=\mathbf{0}$, $\Pi_{\lambda,\mathbf{q},q_\perp}$ is negligible for $\mathbf{q}\neq\mathbf{0}$.

As a consequence of the observations above, we can set $\Pi_{\lambda,\mathbf{q},q_\perp} = \delta_{\lambda,1s}\delta_{\mathbf{q},0}\Pi_{1s,0,q_\perp}$ and use it when we express the source term (34) in the exciton basis. Combining this result with Eq. (B6), we obtain

$$\begin{aligned} i\hbar \frac{\partial}{\partial t}\Delta\langle X^\dagger_{\lambda,\mathbf{q}} X_{\nu,\mathbf{q}}\rangle &= (E_\nu - E_\lambda)\Delta\langle X^\dagger_{\lambda,\mathbf{q}} X_{\nu,\mathbf{q}}\rangle - (E_\nu - E_\lambda) \\ &\quad \times\langle X^\dagger_{\lambda,\mathbf{q}} X_{\nu,\mathbf{q}}\rangle_S + iG^{\lambda,\nu}(\mathbf{q}) + D^{\lambda,\nu}_{\mathrm{rest}}(\mathbf{q}) \\ &\quad + T^{\lambda,\nu}(\mathbf{q}) - 2i\hbar\,\delta_{\mathbf{q},0}[\delta_{\nu,1s}\phi^R_\lambda(\mathbf{r}=\mathbf{0})\Pi_{1s,0,\Sigma} \\ &\quad + \delta_{\lambda,1s}(\phi^R_\nu(\mathbf{r}=\mathbf{0})\Pi_{1s,0,\Sigma})^\star], \end{aligned} \tag{B10}$$

where $\Pi_{1s,0,\Sigma}$ contains the collective photon operator $B_{0,\Sigma}$ defined by Eq. (33). The last term in Eq. (B10) is responsible for the generation of excitons. It shows that only $\mathbf{q}=\mathbf{0}$ excitons are created and that one of the exciton indices has to be $1s$. In addition, the assumed excitation, spectrally at the $1s$ resonance, exclusively generates the exciton population $\Delta\langle X^\dagger_{1s,\mathbf{q}} X_{1s,\mathbf{q}}\rangle$ since all other contributions are nonresonant with the quantum pump and have a smaller $\phi^R_\lambda(\mathbf{r}=\mathbf{0})$ than the $1s$ state.

As a result, only the state

$$\Delta\langle X^\dagger_{\lambda,\mathbf{q}} X_{\nu,\mathbf{q}}\rangle = \delta_{\lambda,\nu}\delta_{\lambda,1s}\delta_{\mathbf{q},0}\Delta\langle X^\dagger_{1s,0} X_{1s,0}\rangle = \delta_{\lambda,\nu}\delta_{\lambda,1s}\delta_{\mathbf{q},0}\Delta N_{1s}(0) \tag{B11}$$

is generated and all other correlations are vanishingly small for resonant quantum excitation. Thus, the essential features of the quantum excitation are described by the closed set of equations

$$\begin{aligned} \frac{\partial}{\partial t}\Pi_{1s,0,q_\perp} &= i\left(\omega_{q_\perp} - \frac{1}{\hbar}E_{1s}\right)\Pi_{1s,0,q_\perp} \\ &\quad - \phi^R_{1s}(\mathbf{r}=\mathbf{0})\Delta\langle B^\dagger_{0,q_\perp} B_{0_\Sigma}\rangle - T^{\Pi}_{\mathbf{k},0,q_\perp}, \end{aligned} \tag{B12}$$

$$\frac{\partial}{\partial t} f_{\mathbf{k}}^{e} = \frac{\partial}{\partial t} f_{\mathbf{k}}^{h} = -2\mathrm{Re}[\Pi_{1s,0,\Sigma}\phi_{1s}^{R}(\mathbf{k})], \tag{B13}$$

$$\hbar \frac{\partial}{\partial t}\Delta\langle X_{1s,\mathbf{q}}^{\dagger} X_{1s,\mathbf{q}}\rangle = -2\delta_{\mathbf{q},0}\mathrm{Re}[\phi_{1s}^{R}(\mathbf{r}=\mathbf{0})\Pi_{1s,0,\Sigma}], \tag{B14}$$

where only those scattering terms have been written that contribute to the generation of excitation.

## APPENDIX C: CLASSICAL AND QUANTUM EXCITATIONS WITH EQUIVALENT INTENSITY CHARACTERISTICS

The position-dependent intensity of the initial pump light, which may be quantum or classical, follows from

$$\langle E(\mathbf{r},z)E(\mathbf{r},z)\rangle_N = \frac{2}{\mathcal{V}}\sum_{\mathbf{q},\mathbf{q}'}\sum_{q_\perp,q_\perp'}\mathcal{E}_q\mathcal{E}_{q'}\langle B_{\mathbf{q},q_\perp}^{\dagger}B_{\mathbf{q}',q_\perp'}\rangle e^{i(\mathbf{q}'-\mathbf{q})\cdot\mathbf{r}}e^{i(q_\perp'-q_\perp)z}, \tag{C1}$$

where the subscript $N$ indicates normal ordering of the operators related to the free-space eigenmodes of light. Also terms $\langle BB\rangle$ and $\langle B^{\dagger}B^{\dagger}\rangle$ are omitted in this expression since they lead to strongly oscillating terms like $e^{i(q_\perp'+q_\perp)z}$ which average to zero as the overall intensity is analyzed. Since the pump is initially propagating freely far away from the planar structure, we use a plane-wave presentation of the modes with a quantization volume $\mathcal{V}=\mathcal{L}\mathcal{S}$ which can be divided into the quantization area $\mathcal{S}$ and length $\mathcal{L}$. For simplicity, we assume homogeneous quantum excitation such that the intensity varies only in the direction perpendicular to the planar structure. Such a dependency is found only if the in-plane momenta of the photon operators match according to $\langle B_{\mathbf{q},q_\perp}^{\dagger}B_{\mathbf{q}',q_\perp'}\rangle = \delta_{\mathbf{q},\mathbf{q}'}\langle B_{\mathbf{q},q_\perp}^{\dagger}B_{\mathbf{q},q_\perp'}\rangle$. This condition implies a generalized incoherent intensity

$$\langle E(\mathbf{r},z)E(\mathbf{r},z')\rangle_N = \langle E(z)E(z')\rangle_N = \frac{2}{\mathcal{V}}\sum_{\mathbf{q},q_\perp,q_\perp'}\mathcal{E}_q\mathcal{E}_{q'}\langle B_{\mathbf{q},q_\perp}^{\dagger}B_{\mathbf{q},q_\perp'}\rangle e^{i(q_\perp'z'-q_\perp z)}, \tag{C2}$$

which depends only on the $z$ coordinate. Applying now the cluster expansion, we find a separation into singlets and doublets

$$\langle E(z)E(z')\rangle_N = \frac{2}{\mathcal{S}}\sum_{\mathbf{q}}\left(\frac{1}{\sqrt{\mathcal{L}}}\sum_{q_\perp}\mathcal{E}_q\langle B_{\mathbf{q},q_\perp}^{\dagger}\rangle e^{-iq_\perp z}\right)\times\left(\frac{1}{\sqrt{\mathcal{L}}}\sum_{q_\perp'}\mathcal{E}_{q'}\langle B_{\mathbf{q},q_\perp'}\rangle e^{iq_\perp' z'}\right) + \frac{2}{\mathcal{S}}\sum_{\mathbf{q}}\left(\frac{1}{\mathcal{L}}\sum_{q_\perp,q_\perp'}\mathcal{E}_q\mathcal{E}_{q'}\Delta\langle B_{\mathbf{q},q_\perp}^{\dagger}B_{\mathbf{q},q_\perp'}\rangle e^{i(q_\perp'z'-q_\perp z)}\right). \tag{C3}$$

For a purely classical field propagating perpendicular to the planar structure only the component $\mathbf{q}=\mathbf{0}$ contributes to the classical factorization. Thus, the excitation intensity in its classical and quantum form is classified by

$$\langle E(z)E(z')\rangle_N \equiv \langle E(z)E(z')\rangle_{\mathrm{classical}} + \langle E(z)E(z')\rangle_{\mathrm{quantum}}, \tag{C4}$$

$$\langle E(z)E(z')\rangle_{\mathrm{classical}} = 2\langle E_0^{\dagger}(z)\rangle\langle E_0(z')\rangle,$$

$$\langle E_0(z)\rangle \equiv \frac{1}{\sqrt{\mathcal{S}\mathcal{L}}}\sum_{q_\perp} i\mathcal{E}_q\langle B_{0,q_\perp}\rangle e^{iq_\perp z}, \tag{C5}$$

$$\langle E(z)E(z')\rangle_{\mathrm{quantum}} = 2\frac{1}{\mathcal{L}\mathcal{S}}\sum_{\mathbf{q},q_\perp,q_\perp'}\mathcal{E}_q\mathcal{E}_{q'}\Delta\langle B_{\mathbf{q},q_\perp}^{\dagger}B_{\mathbf{q},q_\perp'}\rangle e^{i(q_\perp'z'-q_\perp z)}. \tag{C6}$$

In this notation, the initial classical field is defined by $\langle E(z)\rangle=\langle E_0(z)\rangle+\langle E_0^{\star}(z)\rangle$ and it propagates according to the wave equation (13).

For purely classical excitation $\langle E(z)E(z')\rangle_{\mathrm{quantum}}$ vanishes whereas for pure quantum excitation $\langle E(z)E(z')\rangle_{\mathrm{classical}}$ is zero. Since we want to concentrate on the question of how the quantum-statistical aspects of light influence the excitation, we want to make sure that the configurations of the pure quantum and classical excitations are as close to each other as possible with respect to their intensity, temporal, and spectral features. The general form of the intensity Eq. (C4) suggests that we can make the pure quantum and classical excitations nearly identical—apart from their drastic difference in their quantum statistics—by demanding that the initial quantum pulse has the same spatial dependence as its classical counterpart such that

$$\langle E(z)E(z')\rangle_{\mathrm{quantum}} = [2\langle E_0^{\star}(z)\rangle\langle E_0(z')\rangle]_{\mathrm{classical}}. \tag{C7}$$

By taking a Fourier transformation of Eq. (C7) and inserting Eqs. (C5) and (C6) explicitly we find the condition

$$\frac{\mathcal{L}}{\mathcal{S}}\sum_{\mathbf{q}}\mathcal{E}_q\mathcal{E}_{q'}\Delta\langle B_{\mathbf{q},q_\perp}^{\dagger}B_{\mathbf{q},q_\perp'}\rangle = \langle E_0^{\dagger}(q_\perp)\rangle\langle E_0(q_\perp')\rangle,$$

$$\langle E_0(q_\perp)\rangle \equiv \int dz\langle E_0(z)\rangle e^{-iq_\perp z}. \tag{C8}$$

Since this condition can be satisfied by quantum fields that have different distributions of in-plane momenta, we specify the initial condition

$$\mathcal{E}_q\mathcal{E}_{q'}\Delta\langle B_{\mathbf{q},q_\perp}^{\dagger}B_{\mathbf{q},q_\perp'}\rangle = \frac{1}{\mathcal{L}}F(\mathbf{q})\langle E_0^{\dagger}(q_\perp)\rangle\langle E_0(q_\perp')\rangle,$$

$$\frac{1}{\mathcal{S}}\sum_{\mathbf{q}} F(\mathbf{q}) = 1, \tag{C9}$$

where $F(\mathbf{q})$ defines the angular spread of the pure quantum field.

Before the quantum excitation reaches the unexcited semiconductor structure, $\Pi_{\mathbf{k},\mathbf{q},q_\perp}$ and all other carrier excitations vanish. Under such conditions, Eq. (31) can be solved analytically giving $\Delta\langle B^\dagger_{\mathbf{q},q_\perp} B_{\mathbf{q},q'_\perp}\rangle = \Delta\langle B^\dagger_{\mathbf{q},q_\perp} B_{\mathbf{q},q'_\perp}\rangle_0 e^{i(\omega_q-\omega_{q'})t}$. If we assume a narrow angular spread for the quantum excitation, i.e., $F(\mathbf{q}) = \mathcal{S}\delta_{\mathbf{q},0}$, this together with Eq. (C6) produces

$$\begin{aligned}\langle E(z,t)E(z',t)\rangle &= \sum_{q_\perp,q'_\perp} \frac{2\mathcal{E}_q\mathcal{E}_{q'}}{\mathcal{LS}} \Delta\langle B^\dagger_{0,q_\perp} B_{0,q'_\perp}\rangle e^{i(q'_\perp z' - q_\perp z)} = \sum_{q_\perp,q'_\perp} \frac{2\mathcal{E}_q\mathcal{E}_{q'}}{\mathcal{LS}} \mathcal{E}_q\mathcal{E}_{q'} \Delta\langle B^\dagger_{0,q_\perp} B_{0,q'_\perp}\rangle_0 \\ &\quad e^{i[(\omega_q-\omega_{q'})t + (q'_\perp z' - q_\perp z)]} \\ &= \sum_{q_\perp,q'_\perp} \frac{2\mathcal{E}_q\mathcal{E}_{q'}}{\mathcal{LS}} \Delta\langle B^\dagger_{0,q_\perp} B_{0,q'_\perp}\rangle_0 e^{i[q'_\perp(z'-ct) - q_\perp(z-ct)]} = \langle E(z-ct)E(z'-ct)\rangle_{\text{quantum}}.\end{aligned} \tag{C10}$$

Hence, the quantum excitation propagates the same way as the classical one. This observation also shows that choice (C8) provides the same temporal and spectral features for the quantum and the classical excitations since the spatial features of the initial excitation are matched.

## APPENDIX D: QUANTUM STATISTICS OF THE GENERATED STATES

Since the simplified models of the classical and quantum excitation schemes very well describe the nature of the excitation, we use them further to analyze the specific quantum statistics of the quasiparticle excitations before the onset of scattering processes. In particular, we investigate the quantum statistics of the generated excitonic state.

### 1. Quantum statistics of coherent excitons

When the two-particle correlation terms in Eqs. (15)–(17), e.g., the $\Gamma$ term in Eq. (15), can be neglected, these equations are closed and no doublets are involved in the description of the classical excitation. As a result, the system is in the so-called coherent limit [5], where the excitation does not suffer from irreversible decay and we have the strict conservation law

$$\left(f_{\mathbf{k}} - \frac{1}{2}\right)^2 + |P_{\mathbf{k}}|^2 = \frac{1}{4}, \tag{D1}$$

where $f_{\mathbf{k}} \equiv f^e_{\mathbf{k}} = f^h_{\mathbf{k}}$. Since the coherent limit implies that the system does not have correlations, the Hartree-Fock factorization is exact. The resulting wave function is a Slater determinant [25,37]

$$|\Psi_{\text{coh}}(t)\rangle = \prod_{\mathbf{k}} L^\dagger_{\mathbf{k}}(t)|\Psi_0\rangle,$$

$$L^\dagger_{\mathbf{k}}(t) = e^{i\psi_{\mathbf{k}}(t)}\sin\beta_{\mathbf{k}}(t)a^\dagger_{c,\mathbf{k}} + \cos\beta_{\mathbf{k}}(t)a^\dagger_{v,\mathbf{k}}, \tag{D2}$$

where $|\Psi_0\rangle$ is the empty semiconductor without carriers and $L^\dagger_{\mathbf{k}}$ is a fermion creation operator defined by

$$\beta_{\mathbf{k}}(t) = \arcsin\sqrt{f_{\mathbf{k}}}, \quad e^{i\psi_{\mathbf{k}}(t)} = \frac{P_{\mathbf{k}}}{|P_{\mathbf{k}}|}. \tag{D3}$$

Since $f_{\mathbf{k}}$ and $P_{\mathbf{k}}$ can be chosen arbitrarily as long as they obey Eq. (D1), $|\Psi_{\text{coh}}(t)\rangle$ is the exact quantum state after arbitrary classical excitation before the onset of scattering processes.

To find the connection to exciton states, it is convenient to introduce a unitary transformation [25,37],

$$S = \sum_{\lambda} (c^\star_\lambda X_{\lambda,0} - c_\lambda X^\dagger_{\lambda,0}),$$

$$e^S a^\dagger_{v,\mathbf{k}} e^{-S} = e^{i\psi_{\mathbf{k}}(t)}\sin\beta_{\mathbf{k}}(t)a^\dagger_{c,\mathbf{k}} + \cos\beta_{\mathbf{k}}(t)a^\dagger_{v,\mathbf{k}} = L^\dagger_{\mathbf{k}}(t), \tag{D4}$$

which produces the fermionic $L^\dagger_{\mathbf{k}}(t)$ operator after we make the identification

$$e^{i\psi_{\mathbf{k}}(t)}\beta_{\mathbf{k}}(t) \equiv \sum_{\lambda} c_\lambda(t)\phi^R_\lambda(\mathbf{k}). \tag{D5}$$

Consequently, we can use $L^\dagger_{\mathbf{k}}(t) = e^S a^\dagger_{v,\mathbf{k}} e^{-S}$ to express the coherent-limit wave function via

$$\begin{aligned}|\Psi_{\text{coh}}(t)\rangle &= \prod_{\mathbf{k}} (e^S a^\dagger_{v,\mathbf{k}} e^{-S})|\Psi_0\rangle = e^S\left(\prod_{\mathbf{k}} a^\dagger_{v,\mathbf{k}}\right)e^{-S}|\Psi_0\rangle \\ &= e^S \prod_{\mathbf{k}} a^\dagger_{v,\mathbf{k}}|\Psi_0\rangle,\end{aligned} \tag{D6}$$

since $e^S e^{-S} = 1$ and $e^{-S}|\Psi_0\rangle = |\Psi_0\rangle$. We also observe that $\Pi_{\mathbf{k}} a^\dagger_{v,\mathbf{k}}|\Psi_0\rangle \equiv |G\rangle$ is the ground state of a semiconductor where the valence band is completely filled. This allows for a compact form to describe the coherent limit via

$$|\Psi_{\rm coh}(t)\rangle = e^{S}|G\rangle, \tag{D7}$$

which indicates that the operator $e^S$ generates the state related to classical excitations.

A weak resonant classical excitation induces polarization $P_{\mathbf{k}}=p_{1s}\phi^R_{1s}(\mathbf{k})$ having $|p_{1s}|\ll 1$. In this situation,

$$P_{\mathbf{k}} = p_{1s}\phi^R_{1s}(\mathbf{k}), \quad f_{\mathbf{k}} = |p_{1s}\phi_{1s}(\mathbf{k})|^2 + \mathcal{O}(|p_{1s}|^4),$$

$$c_\lambda = \delta_{\lambda,1s}p_{1s} + \mathcal{O}(|p_{1s}|^2), \tag{D8}$$

such that in leading order $|\Psi_{\rm coh}(t)\rangle$ involves only $1s$ excitons. The corresponding generating function and the coherent-limit state then have the forms

$$D_X \equiv e^{S[c]} = e^{p^\star_{1s}X_{1s,0}-p_{1s}X^\dagger_{1s,0}}, \quad |\Psi_{\rm coh}(t)\rangle = D_X|G\rangle, \tag{D9}$$

respectively. Now, the functional form of $D_X$ is identical to that of the displacement operator (10) generating the classical light field when we identify $\beta\leftrightarrow p_{1s}$, $B\leftrightarrow X_{1s}$, and $|0\rangle\leftrightarrow|G\rangle$. Due to this formal analogy, one can say that $|\Psi_{\rm coh}(t)\rangle$ defines *coherent excitons*. Even more so, the quantum statistics of coherent excitons is identical to that of the exciting classical field. However, one should note that the operator $X_{\lambda,0}$ is fundamentally nonbosonic [18] such that $|\Psi_{\rm coh}(t)\rangle$ cannot be interpreted as a bosonic exciton. Moreover, $|\Psi_{\rm coh}(t)\rangle$ is still a Slater determinant of single-electron functions in a conduction-valence-band superposition state. Hence, a coherent exciton is not a truly bound electron-hole pair which must be—by definition—a correlated two-particle electron-hole-pair object.

### 2. Quantum statistics of exciton condensate

The quantum excitation scheme generates an exciton condensate as indicated by Eqs. (40)–(42). Since the scattering terms are irrelevant in this process, we may investigate the quantum statistics of the generated state in its purest form by omitting them completely. In this limit, the singlet-doublet truncation describes the state and its statistics exactly. In this connection, we have direct access to the quantum statistics by solving all possible combinations of exciton operators.

The simplest expectation value follows from

$$\langle X^\dagger_{\lambda,\mathbf{q}}X_{\nu,\mathbf{q}}\rangle = \langle X^\dagger_{\lambda,\mathbf{q}}X_{\nu,\mathbf{q}}\rangle_S + \Delta\langle X^\dagger_{\lambda,\mathbf{q}}X_{\nu,\mathbf{q}}\rangle. \tag{D10}$$

Its singlet contribution can be evaluated with help of Eq. (B7) while the correlated part follows from $\Delta\langle X^\dagger_{\lambda,\mathbf{q}}X_{\nu,\mathbf{q}}\rangle = \delta_{\lambda,\nu}\delta_{\mathbf{q},0}\delta_{\lambda,1s}\Delta N_{1s}(\mathbf{q})$ based on Eq. (39). The singlet part can now be evaluated further by noting that $f^e_{\mathbf{k}}=f^h_{\mathbf{k}}$ are of the order of or smaller than $[a_0^2 n]$, which can be concluded by evaluating $n\equiv(1/\mathcal{S})\Sigma_{\mathbf{k}}f^e_{\mathbf{k}}=[1/(2\pi)^2]\int d^2k\, f^e_{\mathbf{k}}=a^{-2}f^e_0$ for a two-dimensional carrier system where $a^{-1}$ is the typical extension of $f^e_{\mathbf{k}}$ in momentum space. Since $f^e_{\mathbf{k}}$ follows the exciton wave function after the resonant quantum excitation, we may choose $a=a_0$ such that $f^e=\mathcal{O}([na_0^2])$. Thus, we find

$$\langle X^\dagger_{\lambda,\mathbf{q}}X_{\nu,\mathbf{q}}\rangle_S = \sum_{\mathbf{k}}|\phi^L_\lambda(\mathbf{k})|^2 f^e_{\mathbf{k}+\mathbf{q}_e}f^h_{\mathbf{k}-\mathbf{q}_h} \le [na_0^2]^2\sum_{\mathbf{k}}|\phi^L_\lambda(\mathbf{k})|^2 = \mathcal{O}([na_0^2]^2), \tag{D11}$$

which results from Eq. (B7). Using Eq. (D11) in Eq. (D10), we observe that

$$\langle X^\dagger_{\lambda,\mathbf{q}}X_{\nu,\mathbf{q}}\rangle = \delta_{\lambda,\nu}\delta_{\mathbf{q},0}\delta_{\lambda,1s}\Delta N_{1s}(0) + \mathcal{O}([na_0^2]^2). \tag{D12}$$

Here, the quantity $[na_0^2]$ defines how many identical fermionic particles can be found within the typical $1s$-exciton radius $a_0$. Since the quantum excitation leads to singularly large macroscopic $\Delta N_{1s}(0)$, the singlet part appears only as a small correction in the exciton expectation value.

To analyze the quantum statistics, we need to evaluate now the expectation values with all possible combinations of $X_1$ and $X^\dagger_1$. Here, we use the implicit notation where $1\equiv(\lambda_1,\mathbf{q}_1)$ denotes all the relevant exciton indices. Then the general exciton expectation values follow from

$$\langle X^\dagger_1\cdots X^\dagger_J X_K\cdots X_1\rangle = \langle X^\dagger_1\cdots X^\dagger_J X_K\cdots X_1\rangle_{SD}, \tag{D13}$$

which is a $(J+K)$-particle expectation value evaluated via the singlet-doublet truncation. Since the quantum-excitation scheme leads to entirely incoherent dynamics, only incoherent expectation values are nonvanishing. In the case of Eq. (D13) this means that $J$ and $K$ must be equal. Furthermore, e.g., $\langle X_{1s,0}\rangle=p_{1s}$ must vanish since it is directly related to the polarization. Consequently, we only have to analyze the $(2J)$-particle expectation values

$$\langle X^\dagger_1\cdots X^\dagger_J X_K\cdots X_1\rangle = \delta_{J,K}\langle 2J\rangle_{SD} = \delta_{J,K}\sum_{k=0}^{J}\langle 2k\rangle_S\langle 2(J-k)\rangle_D. \tag{D14}$$

After the carrier operators have been normally ordered, we introduced here a formal separation into all possible combinations of pure singlet, $\langle 2k\rangle_S$, and doublet, $\langle 2(J-k)\rangle_D$, terms allowed under incoherent conditions. Since $\langle 2k\rangle_S$ consists of $2k$ singlets which are either $f^e$ or $f^h$, we find a proportionality $\langle 2k\rangle_S=\mathcal{O}([a_0^d n]^{2k})$ where $d$ refers to the dimensionality of the semiconductor system. As a result, Eq. (D14) reduces to

$$\langle X^\dagger_1\cdots X^\dagger_J X_K\cdots X_1\rangle = \delta_{J,K}\langle X^\dagger_1\cdots X^\dagger_J X_K\cdots X_1\rangle_D + \mathcal{O}([a_0^d n]^2), \tag{D15}$$

where only the pure two-particle correlation terms contribute at the lowest order. Clearly, Eq. (D12) obeys this more general relation.

Since the incoherent quantum excitation predominantly populates the state $\Delta\langle X^\dagger_{1s,0}X_{1s,0}\rangle$, we need to consider only index combinations $1=\cdots=J=(1s,0)$. Other combinations can be generated only via scattering and, thus, are of the order $\mathcal{O}([a_0^d n]^2)$. Hence, we use

$$\langle X_1^\dagger \cdots X_J^\dagger X_K \cdots X_1\rangle = \delta_{J,K}\prod_{k=1}^{J}\delta_{k,(1s,0)}\langle [X_{1s,0}^\dagger]^J [X_{1s,0}]^J\rangle_D + \mathcal{O}([a_0^d n]^2). \quad \text{(D16)}$$

To evaluate $\langle [X_{1s,0}^\dagger]^J [X_{1s,0}]^J\rangle_D$, we need to consider all possible factorizations into doublets, which can be separated into two classes: (i) factorizations that do not separate the fermion operators inside any of the exciton operators $X_{1s}$; (ii) the remaining factorizations originating from fermionic exchange terms where one or more fermion operators are exchanged within $X_{1s}=\Sigma_1 \phi_1 a_{v,1}^\dagger a_{c,1}$. Here 1 denotes the carrier momentum and $\phi_1$ the $1s$ exciton wave function.

The part without separation follows from a recursion relation

$$\begin{aligned}\langle X_1^\dagger \cdots X_J^\dagger X_J \cdots X_1\rangle_D^{\text{unbreak}} &= \sum_{k=1}^{J}\Delta\langle X_1^\dagger X_k\rangle\langle X_2^\dagger \cdots X_J^\dagger X_J \cdots X_{k+1}X_{k-1}\cdots X_1\rangle_D^{\text{unbreak}} \\ &= J\Delta N_{1s}(0)\langle [X_{1s,0}^\dagger]^{J-1}[X_{1s,0}]^{J-1}\rangle_D^{\text{unbreak}} \\ &= J!\,[\Delta N_{1s}(0)]^J, \end{aligned} \quad \text{(D17)}$$

as the recursion is performed $J$ times. As a remaining task, we have to evaluate the fermionic exchange terms. The simplest example follows from $\langle [X_{1s,0}^\dagger]^2 [X_{1s,0}]^2\rangle_D^{\text{exc}}$ which among many similar terms has one contribution

$$\begin{aligned}\langle [X_{1s,0}^\dagger]^2 [X_{1s,0}]^2\rangle_D^{\text{exc,one}} &= \sum_{1,2,3,4}\phi_1^\star\phi_2^\star\phi_3\phi_4\Delta\langle a_{c,1}^\dagger a_{c,2}^\dagger a_{v,3}^\dagger a_{v,4}a_{c,4}a_{c,3}a_{c,2}a_{v,1}\rangle_D^{\text{exc,one}} \\ &= -\sum_{1,2,3,4}\phi_1^\star\phi_2^\star\phi_3\phi_4\Delta\langle a_{c,1}^\dagger a_{v,3}^\dagger a_{c,4}a_{v,1}\rangle\Delta\langle a_{c,2}^\dagger a_{v,4}^\dagger a_{c,3}a_{c,2}\rangle \\ &= -\sum_{1,2,3}\phi_1^\star\phi_2^\star\phi_3\phi_3\Delta\langle a_{c,1}^\dagger a_{v,3}^\dagger a_{c,3}a_{v,1}\rangle\Delta\langle a_{c,2}^\dagger a_{v,3}^\dagger a_{c,3}a_{v,2}\rangle \\ &= -\sum_{1,2,3}|\phi_1^\star|^2|\phi_2^\star|^2|\phi_3|^4\Delta N_{1s}(0)\Delta N_{1s}(0) \\ &= -[\Delta N_{1s}(0)]^2\sum_3|\phi_3|^4 \propto [\Delta N_{1s}(0)]^2\frac{a_0^d}{\mathcal{S}}\sum_3|\phi_3|^2 \\ &= -\Delta N_{1s}(0)\frac{\Delta N_{1s}(0)}{\mathcal{S}}a_0^d = \mathcal{O}([na_0^d]), \end{aligned} \quad \text{(D18)}$$

where the third and fourth fermion operators are exchanged. In the evaluation of this term, we have applied the homogeneity (36) and then converted the exciton correlation into the exciton basis via (B4). The final form is obtained by replacing one $|\phi_3|^2$ by its upper limit $|\phi_3|^2 \leqslant a_0^d/\mathcal{S}$ and then using the earlier result (43) implying $\Delta N_{1s}(0)/\mathcal{S}=n$. In general, any exchange of fermion operators leads to a similar proportionality such that overall the fermionic exchange terms scale like $\mathcal{O}([na_0^d])$ which is much smaller than the generated macroscopic population.

By collecting the results (D13)–(D18), we find that quantum excitation seeds a state whose quantum statistics is

$$\langle X_1^\dagger \cdots X_J^\dagger X_K \cdots X_1\rangle = \delta_{J,K}\prod_{k=1}^{J}\delta_{k,(1s,0)}J!\,[\Delta N_{1s}(0)]^J + \mathcal{O}([na_0^d]), \quad \text{(D19)}$$

which shows that for sufficiently low carrier density the quantum excitation scheme generates an exciton condensate with precisely the same statistics as that of the light.


[1] J. J. Hopfield, Phys. Rev. **112**, 1555 (1958).
[2] A. H. Zewail, *Femtochemistry—Ultrafast Dynamics of the Chemical Bond* (World Scientific, Singapore, 1994), Vols. I and II.
[3] U. Hofer, I. Shumay, C. Reuss, U. Thomann, W. Wallauer, and T. T, Science **277**, 1480 (1997).
[4] G. Khitrova, H. M. Gibbs, F. Jahnke, M. Kira, and S. W. Koch, Rev. Mod. Phys. **71**, 1591 (1999).
[5] H. Haug and S. W. Koch, *Quantum Theory of the Optical and Electronic Properties of Semiconductors*, 4th ed. (World Scientific, Singapore, 2004).
[6] D. Lidzey, D. Bradley, M. Skolnick, T. Virgili, S. Walker, and D. Whittaker, Nature (London) **395**, 53 (1998).
[7] F. Wang, G. Dukovic, L. Brus, and T. Heinz, Science **308**, 838 (2005).
[8] A. van Oijen, M. Ketelaars, J. Kohler, T. Aartsma, and J. Schmidt, Science **285**, 400 (1999).
[9] N. Holt, D. Zigmantas, L. Valkunas, X. Li, K. Niyogi, and G. Fleming, Science **307**, 433 (2005).
[10] S. Bellafiore, F. Bameche, G. Peltier, and J. Rochaix, Nature (London) **433**, 892 (2005).
[11] H. J. Kimble, M. Dagenais, and L. Mandel, Phys. Rev. Lett. **39**, 691 (1977).
[12] P. Michler, A. Kiraz, C. Becher, W. Schoenfeld, P. Petroff, L. Zhang, E. Hu, and A. Imamoglu, Science **290**, 2282 (2000).
[13] A. Rauschenbeutel, G. Nogues, S. Osnaghi, P. Bertet, M. Brune, J. Raimond, and S. Haroche, Science **288**, 2024 (2000).
[14] W. Hoyer, M. Kira, S. W. Koch, H. Stolz, S. Mosor, J. Sweet, C. Ell, G. Khitrova, and H. M. Gibbs, Phys. Rev. Lett. **93**, 067401 (2004).
[15] B. Blinov, D. Moehring, L.-M. Duan, and C. Monroe, Nature (London) **428**, 153 (2004).
[16] D. Walls, Nature (London) **306**, 141 (1983).
[17] R. E. Slusher, L. Hollberg, B. Yurke, J. Mertz, and J. Valley, Phys. Rev. Lett. **55**, 2409 (1985).
[18] T. Usui, Prog. Theor. Phys. **23**, 787 (1960).
[19] C. Cohen-Tannoudji, J. Dupont-Roc, and G. Grynberg, *Photons & Atoms*, 3rd ed. (Wiley, New York, 1989).
[20] M. Kira, F. Jahnke, W. Hoyer, and S. W. Koch, Prog. Quantum Electron. **23**, 189 (1999).

[21] H. Wyld and B. Fried, Ann. Phys. (N.Y.) **23**, 374 (1963).
[22] J. Fricke, Ann. Phys. (N.Y.) **252**, 479 (1996).
[23] M. Kira, W. Hoyer, and S. W. Koch, Mol. Cryst. Liq. Cryst. Sci. Technol., Sect. B: Nonlinear Opt. **29**, 481 (2002).
[24] W. Hoyer, M. Kira, and S. Koch, *Cluster Expansion in Semiconductor Quantum Optics*, in Nonequilibrium Physics at Short Time Scales, edited by. K. Morawetz (Springer, Berlin, 2004), pp. 309335
[25] M. Kira and S. Koch, Eur. Phys. J. D **36**, 143 (2005)
[26] F. Jahnke, M. Kira, and S. W. Koch, Z. Phys. B: Condens. Matter **104**, 559 (1997).
[27] A. Thränhardt, S. Kuckenberg, A. Knorr, T. Meier, and S. W. Koch, Phys. Rev. B **62**, 2706 (2000).
[28] M. Kira, W. Hoyer, T. Stroucken, and S. W. Koch, Phys. Rev. Lett. **87**, 176401 (2001).
[29] W. Hoyer, M. Kira, and S. W. Koch, Phys. Rev. B **67**, 155113 (2003).
[30] S. Siggelkow, W. Hoyer, M. Kira, and S. W. Koch, Phys. Rev. B **69**, 073104 (2004).
[31] S. Koch, M. Kira, W. Hoyer, and V. Filinov, Phys. Status Solidi B **238**, 404 (2003).
[32] V. Filinov, W. Hoyer, M. Bonitz, M. Kira, V. Fortov, and S. Koch, J. Opt. B: Quantum Semiclassical Opt. **5**, 299 (2003).
[33] D. F. Walls and G. J. Milburn, *Quantum Optics*, 1st ed. (Springer-Verlag, New York, 1994).
[34] M. Kira, F. Jahnke, and S. W. Koch, Phys. Rev. Lett. **82**, 3544 (1999).
[35] Y.-S. Lee, T. B. Norris, M. Kira, F. Jahnke, S. W. Koch, G. Khitrova, and H. M. Gibbs, Phys. Rev. Lett. **83**, 5338 (1999).
[36] C. Ell, P. Brick, M. Hübner, E. S. Lee, O. Lyngnes, J. P. Prineas, G. Khitrova, H. M. Gibbs, M. Kira, F. Jahnke, S. W. Koch, D. G. Deppe, and D. L. Huffaker, Phys. Rev. Lett. **85**, 5392 (2000).
[37] M. Kira and S. W. Koch, Phys. Rev. Lett. **93**, 076402 (2004).
[38] R. A. Kaindl, M. A. Carnahan, D. Hagele, R. Lovenich, and D. S. Chemla, Nature (London) **423**, 734 (2003).
[39] M. Kira, W. Hoyer, and S. Koch, Solid State Commun. **129**, 733 (2004).
[40] W. Hoyer, C. Ell, M. Kira, S. Koch, S. Chatterjee, S. Mosor, G. Khitrova, H. Gibbs, and H. Stolz, Phys. Rev. B **72**, 075324 (2005).
[41] P. Littlewood, P. Eastham, J. Keeling, F. Marchetti, B. Simons, and M. H. Szymanska, J. Phys.: Condens. Matter **16**, 3597 (2004).
[42] M. Kira, W. Hoyer, S. Koch, Y.-S. Lee, T. Norris, G. Khitrova, and H. Gibbs, Phys. Status Solidi C **0**, 1397 (2003).
[43] S. Chatterjee, C. Ell, S. Mosor, G. Khitrova, H. M. Gibbs, W. Hoyer, M. Kira, S. W. Koch, J. P. Prineas, and H. Stolz, Phys. Rev. Lett. **92**, 067402 (2004).
[44] M. Anderson, J. Ensher, M. Matthews, C. Weiman, and E. Cornell, Science **269**, 198 (1995).
[45] K. B. Davis, M.-O. Mewes, M. R. Andrews, N. J. van Druten, D. S. Durfee, D. M. Kurn, and W. Ketterle, Phys. Rev. Lett. **75**, 3969 (1995).
[46] E. Cornell and C. Wieman, Rev. Mod. Phys. **74**, 875 (2002).
[47] W. Ketterle, Rev. Mod. Phys. **74**, 1131 (2002).
[48] M. Andrews, C. Townsend, H.-J. Miesner, D. Durfee, D. Kurn, and W. Ketterle, Science **275**, 637 (1997).
[49] M. Kasevich, Science **298**, 1363 (2002).
[50] C. Orzel, A. Tuchman, M. Fenselau, M. Yasuda, and M. A. Kasevich, Science **291**, 2386 (2001).
[51] E. T. Jaynes and F. W. Cummings, Proc. IEEE **51**, 89 (1963).
[52] M. Brune, F. Schmidt-Kaler, A. Maali, J. Dreyer, E. Hagley, J. M. Raimond, and S. Haroche, Phys. Rev. Lett. **76**, 1800 (1996).
[53] T. Thiele, *Theory of Observations* (C&E Layton, London, 1903).
[54] V. V. Kocharovsky, V. V. Kocharovsky, and M. O. Scully, Phys. Rev. Lett. **84**, 2306 (2000).